NASA CONTRACTOR
REPORT

NASA CR-1845

NASA CR-1
C.1

THE CALCULATION OF
THREE-DIMENSIONAL TURBULENT
BOUNDARY LAYERS ON HELICOPTER ROTORS

by J. G. Hicks and J. F. Nash

Prepared by
LOCKHEED GEORGIA RESEARCH LABORATORY
Marietta, Ga.
for Ames Research Center

NATIONAL AERONAUTICS AND SPACE ADMINISTRATION • WASHINGTON, D. C. • MAY 1971

1. Report No. NASA CR-1845	2. Government Accession No.	3. Recipient's Catalog No.
4. Title and Subtitle The Calculation of Three-Dimensional Turbulent Boundary Layers on Helicopter Rotors		5. Report Date May 1971
		6. Performing Organization Code
7. Author(s) J. G. Hicks and J. F. Nash		8. Performing Organization Report No.
		10. Work Unit No.
9. Performing Organization Name and Address Lockheed Georgia Research Laboratory Marietta, Georgia		11. Contract or Grant No. NAS 2-5652
		13. Type of Report and Period Covered Contractor Report
12. Sponsoring Agency Name and Address National Aeronautics & Space Administration Washington, D.C. 20546		14. Sponsoring Agency Code

15. Supplementary Notes

16. Abstract

The three-dimensional turbulent boundary layer on a helicopter rotor was investigated analytically. The method of Nash, which takes into account crossflows and crossflow derivatives, was modified to include the effects of centrifugal and Coriolis forces. The technique was quasi-steady in the sense that the blade was assumed to be "frozen" at any given azimuthal position. Calculations were performed on an NACA 0012 section and an advanced airfoil for a range of azimuthal positions and two advance ratios. Cases were also run in which (1) spanwise derivatives, and (2) spanwise velocities and derivatives were neglected, corresponding to flows over infinite yawed wings and to two-dimensional flows, respectively. For cases where the rotor was at high incidence, the calculation method predicted early separation. Investigations of this condition led to the conclusion that the omission of the effects of time-dependence was probably responsible for the pessimistic estimates of the separation boundaries.

17. Key Words (Suggested by Author(s)) Turbulent Flow Calculation Three Dimensional Boundary Layers Helicopter Rotor Retreating Blade Stall	18. Distribution Statement UNCLASSIFIED-UNLIMITED	
19. Security Classif. (of this report) UNCLASSIFIED	20. Security Classif. (of this page) UNCLASSIFIED	21. No. of Pages 66 — 22. Price* 3.00

CONTENTS

THE CALCULATION OF THREE-DIMENSIONAL

TURBULENT BOUNDARY LAYERS ON HELICOPTER ROTORS

By J. G. Hicks and J. F. Nash
Lockheed Georgia Research Laboratory

SUMMARY

The three-dimensional turbulent boundary layer on a helicopter rotor was investigated analytically. The method of Nash, which takes into account crossflows and crossflow derivatives, was modified to include the effects of centrifugal and Coriolis forces. The technique was quasi-steady in the sense that the blade was assumed to be "frozen" at any given azimuthal position. Calculations were performed on an NACA 0012 section and an advanced airfoil for a range of azimuthal positions and two advance ratios. Cases were also run in which (1) spanwise derivatives, and (2) spanwise velocities and derivatives were neglected, corresponding to flows over infinite yawed wings and to two-dimensional flows, respectively. For cases where the rotor was at high incidence, the calculation method predicted early separation. Investigations of this condition led to the conclusion that the omission of the effects of time-dependence was probably responsible for the pessimistic estimates of the separation boundaries.

INTRODUCTION

The rotor of a helicopter in forward flight experiences a time-dependent, highly three-dimensional flow environment. In contrast, typical design calculations involve a number of simplifying assumptions, the most important of which are:

- that the blade can be frozen at some particular azimuthal position, and the effects of time-dependence ignored

- that the effects of three-dimensionality in the boundary layer can be ignored, and the flow treated by two-dimensional strip theory.

Since there is considerable concern about the soundness of these assumptions, one of the present objectives of helicopter research is to assess their validity. McCroskey and Yaggy (ref. 1) and Dwyer and McCroskey (ref. 2) have made an extensive study of the effects of time-dependence and three-dimensionality on the laminar boundary layer on a rotor. The work reported here related to the turbulent boundary layer on a helicopter rotor and had the following objectives:

(a) Demonstrate that fully three-dimensional calculations of the turbulent boundary layer on a rotor can be performed using state-of-the-art technology.

(b) Generate a set of reference data covering a range of representative rotor conditions for a standard and an "advanced" rotor design.

(c) Assess the effect on the calculations of ignoring either spanwise (radial) derivatives in the boundary layer, or spanwise derivatives and velocities; typical design calculations correspond to the latter.

It is the intention to carry out a further study of the effects of time-dependence on the turbulent boundary layers at a later date; these effects are ignored in the present work.

Part 1 of this report deals with the work which addressed these objectives over the greater part of the contract period. However, during the course of performing the calculations aimed at objective (b), it was noticed that early separation of the boundary layer (i.e., stall) was predicted to occur for a wider range of conditions than has been observed experimentally in either wind-tunnel or flight tests. Therefore, some additional calculations were made in an attempt to determine the cause of this disparity. These latter calculations are discussed in Part 2 of the report.

SYMBOLS

a_1, a_2	constants in turbulent energy equation
c	chord length
L	dissipation length
p	static pressure
q	resultant velocity
R	rotor blade radius
Re	Reynolds number
$S_1, \ldots S_5$	Weber tabulated functions
t	time
T	integrated skin friction, $\displaystyle\int_{x_o}^{x} \tau_w \cos\theta \, dx$
u	chordwise velocity
$\bar{u}$	2-D velocity distribution
V_∞	translational velocity of rotor
w	spanwise velocity
x	distance measured in chordwise direction
y	distance measured normal to wall

z	distance measured in spanwise direction
α	angle of attack
δ	boundary-layer thickness
δ^*	boundary-layer displacement thickness
θ	shear stress angle relative to x-axis
μ	advance ratio, $V_\infty/\Omega R$
ν	kinematic viscosity
ρ	density
τ	shear stress
ψ	azimuthal angle
Ω	rotational velocity

Subscripts

e	value at the outer edge of boundary layer
x, z	component in x- and z-direction
w	value at wall
∞	freestream value at infinity
o	value at start of turbulent boundary layer

Part 1

Basic Parametric Studies

OUTLINE OF THE METHOD

The problem consisted of calculating the three-dimensional turbulent boundary layer on a translating rotor, given the local incidence of the blade, as a function of spanwise (radial) and azimuthal positions, the tip velocity, and the advance ratio. The calculation was handled in two stages: the pressure distribution over the blade was first derived, and then the boundary-layer development was computed using this pressure distribution (Figure 1).

The pressure distribution was calculated by two-dimensional strip theory. The method of Weber (refs. 3 and 4 and unpublished work) was used to derive the pressure distribution over each section of the blade, in terms of the airfoil geometry and the local angle of incidence, assuming two-dimensional flow at the local relative speed of the blade $(\Omega z + V_\infty \sin \psi)$ (see figure 2), and the appropriate Mach number. The local pressure coefficient at a point on the blade was converted to a velocity by the exact form of Bernoulli's equation for compressible flow, and this velocity was used as a boundary condition for the calculation of the turbulent boundary layer. (The method of Weber is described in more detail under the section on "Potential Flow Method" below.)

The turbulent boundary layer was calculated by the method of Nash (ref. 5) modified by the inclusion of rotation terms in the momentum equations. The method consists of a coupled integration of the time-averaged equations of motion and the empirically modified turbulent-energy equation. The method is three-dimensional with respect to both spanwise velocities and shear stresses, and spanwise derivatives. The boundary-layer calculation was performed as though the flow were locally incompressible, using the compressible, potential-flow velocity distribution. (The boundary-layer method is described in more detail under the section on "Calculation of the Boundary Layer" below.)

POTENTIAL-FLOW METHOD

The boundary-layer method requires the specification of the surface pressure distribution over the region ABCD in figure 3. This was calculated by two-dimensional strip theory, given the section geometry and the local angle of incidence at a number of spanwise (z-) stations. The latter data were inferred from measured loading distributions on an actual rotor, and were supplied to Lockheed by the Technical Monitor. The method of Weber was used (refs. 3 and 4 and unpublished work) to generate the appropriate two-dimensional pressure distributions. This method combines the classical singularity-distribution technique with a conformal transformation. The singularities are distributed along the chordline, as in linear airfoil theory, but a correction is made near the leading edge based on the exact solution for an ellipse. The method is applicable to arbitrarily shaped sections and is considered to be among the most reliable for its degree of sophistication.

The boundary-layer method is presently restricted to incompressible flow. However, the pressure distributions were derived for compressible flow, and the boundary-layer calculations were done as though the flow were locally incompressible. In the version of the Weber method which was used, a semi-empirical compressibility correction is included which gives a fairly accurate representation of the effects of increasing Mach number up to the critical Mach number.

The basic equation in the Weber method is

$$\frac{u}{u_\infty} = \frac{\left[1 + S_1(x) \pm S_4(x)\right] \cos\alpha \pm \sqrt{\frac{1-x}{x}}\left(1 + S_3(x)\right) \sin\alpha}{\sqrt{\left[1 + \left(S_2(x) \pm S_5(x)\right)^2\right]}} \tag{1}$$

4

where the values of S_N are functions of airfoil geometry, and of Mach number; for incompressible flow they are defined as follows:

$$S_1(x) = \frac{1}{\pi} \int_0^1 \frac{dy}{dx} \frac{d\overline{x}}{x - \overline{x}} \tag{2}$$

$$S_2(x) = \frac{dy}{dx} \tag{3}$$

$$S_3(x) = \frac{1}{\pi} \int_0^1 \left[\frac{dy}{dx} - \frac{2y(\overline{x})}{1 - (1 - 2\overline{x})^2} \right] \frac{d\overline{x}}{x - \overline{x}} \tag{4}$$

$$S_4(x) = \frac{1}{\pi} \sqrt{\frac{1-x}{x}} \int_0^1 \frac{dz}{d\overline{x}} \sqrt{\frac{\overline{x}}{1-\overline{x}}} \frac{d\overline{x}}{x - \overline{x}} \tag{5}$$

$$S_5(x) = \frac{dz}{dx} \tag{6}$$

where y and z are the thickness and camber coordinates, respectively.*

The section shape of the NACA 0012 airfoil, which was used in most of the calculations, is defined by

$$\pm y = \frac{0.12}{0.20} \left(0.29690\sqrt{x} - 0.12600x - 0.35160x^2 + 0.28430x^3 - 0.10150x^4 \right) \tag{7}$$

The airfoil has a small, but finite, trailing-edge thickness, and this caused a difficulty in applying the Weber potential-flow method; the method assumes that the trailing edge is sharp. To overcome this difficulty the section geometry was modified by reducing the vertical coordinates by x/c times the trailing-edge thickness. The modification only affects the pressure distribution in the trailing-edge region, and in this region the calculated pressure distribution is discarded anyway and replaced by a faired one which removes the potential-flow stagnation point.

---

*The authors are indebted to T. H. Moulden of the Aerospace Sciences Laboratory (presently on leave at the University of Tennessee Space Institute) for his development of the computer program for calculating the potential-flow pressure distributions.

CALCULATION OF THE BOUNDARY LAYER

Governing Equations

In the notation of Dwyer and McCroskey (ref. 2), the momentum equations for the boundary layer on a translating helicopter rotor, in incompressible flow, are

$$\frac{\partial u}{\partial t} + u \frac{\partial u}{\partial x} + v \frac{\partial u}{\partial y} + w \frac{\partial u}{\partial z} - 2\Omega w \cos\alpha = \frac{\partial \tau_x}{\partial y} + \Omega^2 x - \frac{\partial p}{\partial x} \tag{8}$$

$$\frac{\partial w}{\partial t} + u \frac{\partial w}{\partial x} + v \frac{\partial w}{\partial y} + w \frac{\partial w}{\partial z} + 2\Omega u \cos\alpha = \frac{\partial \tau_z}{\partial y} + \Omega^2 z - \frac{\partial p}{\partial z} \tag{9}$$

where α is the angle between the blade surface and the plane of the rotor disc. The coordinate system (x,y,z) rotates with the blade (Figure 2) at an angular velocity Ω. In a quasi-steady analysis some approximation has to be made to the time-dependent terms $\partial u/\partial t$ and $\partial w/\partial t$. These terms cannot (as sometimes has been assumed) simply be discarded because, even at the edge of the boundary layer on a rotating flat plate, they are equal to $\Omega V_\infty \cos\psi$ and $-\Omega V_\infty \sin\psi$, respectively, where V_∞ is the translational speed of the rotor, and are comparable in magnitude to the remaining terms. However, if it can be assumed that

$$\frac{\partial}{\partial t}(u_e - u) \ll \frac{\partial u_e}{\partial t} \tag{10}$$

$$\frac{\partial}{\partial t}(w_e - w) \ll \frac{\partial w_e}{\partial t} \tag{11}$$

which is valid at least in the outer part of the boundary layer, their dependence on y can be neglected, and the time-dependent terms can be regarded as a sort of additional pressure gradient; specifically, it is permissible to write

$$\frac{\partial p}{\partial x} + \frac{\partial u}{\partial t} = \Omega^2 x - u_e \frac{\partial u_e}{\partial x} - w_e \frac{\partial w_e}{\partial x} \tag{12}$$

$$\frac{\partial p}{\partial z} + \frac{\partial w}{\partial t} = \Omega^2 z - u_e \frac{\partial u_e}{\partial z} - w_e \frac{\partial w_e}{\partial z} \tag{13}$$

In equations (12) and (13), the following substitution has been made:

$$\frac{\partial u_e}{\partial z} + \frac{\partial w_e}{\partial x} = 2\Omega\cos\alpha \tag{14}$$

where $2\Omega\cos\alpha$ is the apparent vorticity in the rotating coordinate system x,y,z.

According to the method of Nash (ref. 5), the magnitude of the turbulent shear stress, τ, is determined from the empirically modified turbulent-energy equation

$$\frac{1}{2a_1}\left(\frac{\partial \tau}{\partial t} + u\frac{\partial \tau}{\partial x} + v\frac{\partial \tau}{\partial y} + w\frac{\partial \tau}{\partial z}\right) = \tau_x\frac{\partial u}{\partial y} + \tau_z\frac{\partial w}{\partial y} - \frac{\tau_{max}}{q_e}\frac{\partial}{\partial y}(a_2\tau) - \frac{\tau^{3/2}}{\rho^{1/2}L} \qquad (15)$$

where a_1 is taken to be a universal constant (=0.15), and a_2 and L are universal functions of y/δ. τ_x and τ_z are the components of τ in the x- and z-directions, respectively, such that

$$\tau_x^2 + \tau_z^2 = \tau^2 \qquad (16)$$

and the assumption is made that the shear stress acts in the direction of the mean rate of strain:

$$\tau_x \Big/ \left(\frac{\partial u}{\partial y}\right) = \tau_z \Big/ \left(\frac{\partial w}{\partial y}\right) \qquad (17)$$

It will be noted that there are no Coriolis or centrifugal terms in equation (15). This is consistent with the fact that $\tau/2a_1$ (which takes the place of the turbulent kinetic energy) is a scalar. However, the assumption is implicit that the structure of the turbulence is unaffected by the streamline curvature. At the edge of the boundary layer, where τ falls to zero, there is no influence of the time-dependence; within the layer, $\partial \tau/\partial t$ is finite, but it has been neglected in the present work.

Boundary Conditions

At the edge of the boundary layer, the chordwise and spanwise components of velocity are given approximately by

$$\left. \begin{array}{l} u_e = (\Omega z + V_\infty \sin \psi)\bar{u} \\[2mm] w_e = -\Omega x + V_\infty \cos \psi \end{array} \right\} \qquad (18)$$

where ψ is the azimuthal angle and $\bar{u}$ is the dimensionless, two-dimensional speed distribution about that section of the blade. The function $\bar{u}(x)$, at each value of z, was calculated according to potential-flow theory by the method described in the preceding section on "Potential-Flow Method."

The boundary-layer calculations were started at a transition "line" (BC, in Figure 3) which was assumed to lie parallel to the leading edge of the blade at a value of x corresponding to the furthest forward position of the suction peak over the range of z of interest ($0.6 \leq z/R \leq 0.9$). The transition "line" was never allowed to lie further downstream than 10-percent chord, and most of the lower-surface calculations start at that position. The assumed location of the transition "line" for each case is indicated in table I. At the transition "line" the turbulent boundary layer was assumed to be of flat-plate form, and of thickness δ such that the Reynolds number, $u_e\delta/\nu$, was equal to 3000: a typical value at the end

7

of transition on a flat plate. The velocity and shear-stress profiles were assumed to be collateral but aligned at the local angle of the external flow.

The boundary conditions along AB and CD (Figure 3) are known even less precisely. In principle, for the side AB, for example, the boundary conditions affect the flow in a region bounded by AB and the streamline through B (or, more precisely, the stream surface passing through the normal to the blade surface at B). When the streamline through B lies outside the region ABCD, the problem does not arise, and the specification of boundary conditions along AB is unnecessary; however, when it lies inside, boundary conditions are formally required, and since these cannot be provided in practice, some suitable (if strictly invalid) procedure must be adopted just to permit the calculation to continue. In the present calculations, the z-derivatives along the side of the domain in question, which properly provide the mechanism for the transfer of information into the domain from outside, were calculated from known quantities inside the domain. Sometimes this procedure leads to numerical instability, but in the present case it did not, and the results are submitted here together with the cautionary statement that computed values at either $z/R = 0.6$ or $z/R = 0.9$, depending on the sign of w_e, may be less reliable than the remainder of the data. Values at $z/R = 0.6$ are generally suspect near $\psi = 0$, and values at $z/R = 0.9$ near $\psi = 180°$.

Calculations Assuming Two-Dimensional or Infinite-Yawed-Wing Flow

Equations (8) through (18) plus continuity define the governing equations for the fully three-dimensional case, and these equations were used in the calculations referred to as "standard calculations" under "Presentation of Results" below. Two sets of comparison calculations were also performed to determine the effects of making additional simplifying assumptions.

In the first set, the assumption was made that the boundary layer corresponded to that on an infinite yawed wing.* Specifically, the terms involving $\partial u/\partial z$, $\partial w/\partial z$ in equations (8) and (9), respectively, were omitted in these calculations, and an appropriate adjustment was made to the pressure gradients to recover the correct variation of u_e and w_e with x. The Coriolis and centrifugal terms in equations (8) and (9) were retained. It will be noted that, although the derivatives of u and w with respect to z are omitted, $\partial p/\partial z$ must be retained to balance the centrifugal forces. The analogy with the flow on an infinite yawed wing is not, therefore, a precise one. However, these calculations were considerably simpler than those that were fully three-dimensional. Coupling between the flow at different z-stations was eliminated, and the calculations could be done for one z-section independently of the rest of the blade.

In the second set, the spanwise component of the velocity, w, was omitted throughout, reducing the equations to two-dimensional form. Equation (8) is the only momentum equation remaining, and this does not now contain a Coriolis term; the centrifugal term also vanishes by virtue of equation (12).

---

*These calculations will be referred to as "yawed-wing" calculations throughout this report. Conventional, non-rotating wings, whose leading edges are other than perpendicular to the flight direction, are referred to as "swept wings" or "infinite swept wings" as the case may be.

Method of Solution

The boundary-layer development is completely specified by the two momentum equations (equations 8 and 9), the shear-stress equation (equation 15), the continuity equation, and the various boundary conditions. The equations were integrated in a three-dimensional domain extending from $z/r = 0.6$ to $z/R = 0.9$, in the spanwise direction, and from the blade surface to a height 25-percent greater than the maximum boundary-layer thickness at the particular x-station (the height of the domain varied with x). The calculation proceeded from the assumed position of the transition "line" to the trailing edge, or to the earliest point at which separation occurred. Separation is defined here as the condition where the chordwise component of skin friction falls to zero. The numerical scheme used was identical to that described in reference 5.

Fifteen collocation points were used in the y-direction, and five in the z-direction; the number of x-steps varied from one case to another, but was of order 2000.

PRESENTATION OF RESULTS

Upon completion of the program development, a number of test cases were performed, for a flat-plate rotor and for a rotor with an elliptic airfoil section, to determine whether the computer program was working correctly. It was considered particularly important to check the validity of the momentum equations which had been modified to take account of the Coriolis and centrifugal forces. The flat-plate rotor provided a simple means of doing this, since for this case, the pressure is constant everywhere, and the potential-flow velocity distribution over the rotor disc is given by simple analytic functions. Interest later developed in the flat-plate-rotor calculations in their own right, and a paper was written describing them (ref. 6).

Most of the calculations referred to here were performed for the Sikorsky H-34 rotor for which both wind-tunnel and flight test data are available (refs. 7 and 8, respectively). The rotor has the following characteristics:

> NACA 0012 airfoil section
> $R = 28$ feet
> $c = 1.37$ feet

Some comparison calculations were also done for a rotor with the same blade chord and radius but with a different airfoil section. One of the advanced airfoils (23010 Modified) currently being evaluated at the U. S. Army Aeronautical Research Laboratory was used. Two advance ratios were considered, equal to 0.23 and 0.45, each corresponding to a particular tip velocity:

> $\Omega R = 566$ ft./sec. for $\mu = 0.23$
>
> $\Omega R = 650$ ft./sec. for $\mu = 0.45$

A standard atmosphere, corresponding to conditions at sea level, was assumed in the calculations.

The calculations performed were as follows:

| | Standard Calculations | | | | Two-Dimensional |
ψ	NACA 0012 $\mu = .23$	NACA 0012 $\mu = .45$	Adv. Airfoil $\mu = .23$	Yawed Wing $\mu = .45$	$\mu = .45$
0	U	U & L	U	U & L	U
90°	U	U & L	U		U
180°	U	U & L	U		U
210°		U			
240°		U & L		U & L	U
270°	U	U & L	U		
300°	U	U			
330°		U			

U = upper surface
L = lower surface

The "standard calculations" were those in which the fully three-dimensional equations were integrated; the "yawed-wing" and "two-dimensional" calculations were those in which either spanwise derivatives or spanwise derivatives and velocities were ignored (see "Calculation of the Boundary Layer").

For each "case," the chordwise and spanwise velocity profiles were calculated at the stations: $x/c = 0.1$, 0.3, 0.6 and 0.9; $z/R = 0.6$, 0.75, and 0.9. At the three spanwise stations, the variation of local skin friction (magnitude and direction) was determined, and also the integrated chordwise component of skin friction (which is associated with the torque on the rotor). The calculation continued to the trailing edge, or to the most upstream point at which separation occurred. The results are summarized in table I.

Table I shows, for each case, the value of x/c at which the calculation started (i.e., the assumed position of the "transition line"), the separation point, if any, the integrated chordwise skin friction, T, and the variation of the boundary-layer thickness, δ, with x and z. Values of u_e, w_e are also given for reference. T is made nondimensional by division by $\rho V_\infty^2 c$, and the velocities u_e, w_e by division by V_∞. In some cases, where early separation was observed when the calculation was started at the suction peak, a second calculation was run starting at a position further downstream. Data corresponding to these auxiliary calculations are shown in brackets.

Figures 4 and 5 illustrate the shape of the calculated profiles on the blade for an azimuthal angle $\psi = 0$. Here the velocities, u,w, are nondimensionalized by division by q_e, the local resultant velocity at the edge of the boundary layer, and y by division by δ. There is nothing remarkable about these profiles; the chordwise profiles (figure 4) respond to the progressive retardation of the flow associated with the chordwise pressure distribution, by becoming less "full," while the spanwise profiles (figure 5) vary somewhat less with chordwise

position but in the direction of increasing "fullness." This behavior is similar to that of the boundary layer on an infinite swept wing (ref. 9). Figure 6 shows the chordwise variation of the resultant skin friction, τ, and the angle, θ, between the limiting streamline and the x-axis. From top to bottom the curves of τ are in the order: $z/R = 0.6$, 0.75, and 0.9, respectively, while the curves of θ are in the reverse order. The skin friction is nondimensionalized by division by ρV_∞^2. It should be noted that θ is generally not equal to the conventionally defined wall-crossflow angle because the external streamlines are generally not parallel to the x-axis. At a separation point, θ tends to $90°$ but the value of the skin friction generally remains finite.

DISCUSSION OF RESULTS

The first objective of this work was to demonstrate that calculations of the three-dimensional turbulent boundary layer on a helicopter rotor could be performed using existing technology, or at least by adapting available methods. The data presented in table I and figures 4, 5, and 6 show that this objective has been attained, although as was stated in the Introduction, some disagreement between the calculations and observation is apparent with regard to separation onset. Figure 7 shows the portion of the blade disc over which separation is predicted to occur forward of 50-percent chord, for at least one radial station of the blade. This figure corresponds to the results for the NACA 0012 section at an advance ratio $\mu = 0.45$; the results for $\mu = 0.23$ are sill more pessimistic. Experimentally, early separation, or stall, is observed over a considerably smaller portion of the disc, and attempts were subsequently made to determine the reasons for the discrepancy. (This question will be discussed in Part 2 of this report.)

Another major goal of the work was to assess the effects of three-dimensionality in the turbulent boundary layer on the rotor, and to determine the errors arising from the application of strip theory. This question can be answered on the basis of the results obtained under conditions where attached flow is predicted over most of the chord. Figure 8 shows a comparison of the skin-friction results from the standard calculations, the "yawed-wing" calculations, and the two-dimensional calculations. The values of τ predicted according to two-dimensional strip theory are roughly 25 percent too low around the mid-chord position. However, it should be remembered that this two-dimensional skin friction would act in the chordwise direction; compared with the chordwise component of the three-dimensional τ, it is too high.* Separation is also predicted to occur too far downstream. The "yawed-wing" calculations yield significantly better results. Both the magnitude and the direction of the skin friction are predicted in close agreement with the standard calculations, and the separation position is predicted accurately; within one percent of the value of x/c given by the standard calculations.

Thus, these calculations suggest that two-dimensional strip theory is satisfactory as far as order-of-magnitude predictions are concerned, but is lacking in precision. "Yawed-wing"

---

*On infinite swept wings, also (i.e., nonrotating ones, not to be confused with the "yawed-wing" calculations referred to in this report), two-dimensional calculations of skin friction yield values which lie between the true resultant skin friction and its chordwise component (ref. 9).

calculations are in excellent agreement with fully three-dimensional calculations, and accordingly, there seems little point in carrying out expensive three-dimensional calculations if data are only required at one z-station. Of course, if data are required over some finite part of the span, there would be little gain. The fact that the inclusion of the spanwise derivatives has a negligible effect on the calculations is perhaps to be expected as a result of the high aspect ratio of the blades.

Part 2

Extended Analyses

PESSIMISTIC SEPARATION PREDICTIONS

Various suggestions can be made with regard to the disagreement between the predicted and the observed onset of separation. The present discussion is based on the premise that the experimental observations are correct (or correctly interpreted) and that, for some reason, the theoretical predictions are pessimistic. There are strong reasons for assuming that this premise is valid, although the contrary cannot altogether be ruled out.

The following possible inadequacies of the calculations have been mentioned:

(a)   The assumed local angles of incidence of the blade are too high.

(b)   The pressure distributions are predicted incorrectly.

(c)   The boundary layer calculations start too far forward on the blade.

(d)   The starting conditions assumed for the boundary-layer calculation are incorrect.

(e)   The calculation method itself is deficient under the conditions existing on the blade (large adverse pressure gradients, etc.).

(f)   The quasi-steady approach is inadequate for dealing with such highly time-dependent flows.

The angles of incidence were obtained from an examination of the measured blade loading in the neighborhood of the leading edge, and therefore they contain a built-in correction for viscous effects. The pressure distributions obtained from the Weber method, using these angles of incidence, have been compared with the measured loading distributions, and no inconsistencies were apparent. The predicted pressure distributions for the NACA 0012 blade also agreed well with the tabulations of reference 10. At the high angles of attack involved, as high as 18° in some cases, a leading-edge (laminar) separation bubble might be expected, but the experimental loading distributions gave no clear indication of it. Any alleviation of the high suction peaks, resulting from the existence of a bubble, would, of course, relieve the strong adverse pressure gradients and would, therefore, have a major effect on the subsequent onset of turbulent separation.

12

The predicted separation position was found to depend strongly on the point at which the calculation was started. However, in the absence of a bubble, there would be no reason to expect transition to occur far downstream of the suction peak; the laminar boundary layer would simply separate if it did. Nor is it likely that transition would take place forward of the suction peak; the leading-edge radius of the blade and the effective angles of sweep are too small for contamination of the laminar flow to occur on the attachment line, and transition is even more unlikely in the region of high favorable pressure gradient just downstream of the leading edge.

With regard to possibility (e), it must be conceded that the turbulent boundary-layer method has not been checked extensively in three-dimensional flows approaching separation. However, in equivalent two-dimensional flows, the method (which then reduces to the method of ref. 11) is known to be accurate and reliable, as the Stanford Conference testifies. Nor are the pressure gradients on the blade excessively severe; even in those cases where separation takes place forward on the blade, the turbulent boundary layer remains attached for a distance corresponding to many times its initial thickness. In short, it would not appear that the boundary layer on the blade is in any sense an unusual one, that is, except for its time-dependent character which has not been considered here. There is a strong possibility that the effects of time-dependence, which have been ignored in the present calculations, could indeed account for the discrepancy between the calculated and the observed separation boundaries. This possibility draws attention to the urgency of proceeding to the next stage of the work, which is to examine the unsteady features of the rotor boundary layer.

The remainder of the present work was aimed at examining the sensitivity of the calculations to changes of the initial boundary-layer thickness. To see whether this sensitivity was greater than it would be in a two-dimensional flow, some calculations were also done for a two-dimensional airfoil at a high angle of attack. A case was chosen for which experimental data were available, and the comparison with these data affords further confirmation of the reliability of the basic method under conditions similar in some respects to those on the blade.

With regard to the initial conditions for the turbulent boundary-layer calculation, it should be remembered that the real boundary layer starts at some imprecisely defined station toward the end of a transition region, and that this transition region is located near a high suction peak. A laminar separation bubble may also be present. It is clear that, with available technology, the velocity and shear-stress profiles at the start of the turbulent boundary layer cannot be predicted with any degree of certainty, either theoretically or by semi-empirical methods. Indeed, it is not even possible to estimate the boundary-layer thickness. In the present work, a necessarily gross assumption has been made about the initial value of δ. The assumption was that the Reynolds number based on δ was equal to 3000, a value which is considered to be about the minimum for fully developed turbulent flow on a flat plate. There is no evidence to suggest that this minimum should be either greater or less under conditions corresponding to the rotor blade.

SENSITIVITY OF THE METHOD TO STARTING CONDITIONS

Some two-dimensional calculations were done for an NACA 63-009 airfoil at 8.5° incidence, to compare the results with the experimental data of McCullough and Gault (ref. 12). The measured chordwise pressure distribution was used, and the measured boundary-layer thickness and velocity profile at x = 0.006c were fed in as starting conditions. The experimental data did not include shear-stress measurements, and the shear-stress profile at the initial station was assumed to be of flat-plate form. At 8.5° incidence, the airfoil develops a high suction peak, similar to that on the rotor, and in the real flow, a small laminar separation bubble occurred at the leading edge, with reattachment taking place a short distance ahead of the x = 0.008c station. Reattaching boundary layers usually have a higher average level of shear stress than do those which have not separated, and the assumed flat-plate profile probably represented an underestimate of the average shear stress at the initial station. The calculations were conservative to this extent; they would tend to predict a slightly earlier separation than would be the case if the initial shear stresses had been represented correctly.

Indeed, the calculations indicated separation at x = 0.93c, whereas the actual flow was observed to remain attached over the whole chord. However, the predicted variation of displacement thickness, δ^*, with x/c was found to be in good agreement with experiment (figure 9).

Some further calculations were performed for the same airfoil to see whether variation of the initial boundary-layer thickness had any significant effect on the predicted separation position, and this proved to be so. Figure 10 shows that, as the initial boundary-layer thickness was progressively increased above the measured value, a point was reached beyond which the separation point moved rapidly upstream to a position close to the leading edge.

This result appeared to lend support to the suggestion that the initial boundary-layer thickness assumed in the rotor calculations was too large, and that the premature separation might not occur if it were reduced. However, this was not the case. With the initial value of δ corresponding to R_δ = 3000, separation on the rotor,* at ψ = 240°, occurred at x = 0.02c; reduction of this value of δ by as much as a factor of one thousand delayed separation to only 0.04c. The rather surprising difference in behavior between the rotor and the two-dimensional airfoil was traced to differences in the chordwise variation of the potential-flow velocity gradients. Figure 11 shows the variation with x/c of the quantity

$$\frac{c}{u_e} \frac{\partial u_e}{\partial x}$$

which is a measure of the local effective chordwise velocity gradient. Regions in which this gradient is large are critical regions for determining whether the boundary layer will separate. In the case of the two-dimensional airfoil, the gradient is a maximum at the initial station; hence, manipulation of the starting conditions is likely to have a significant effect on separation, as is the observed fact. In the case of the rotor, however, the maximum gradient occurs some distance downstream of the initial station, and separation is

---

*Standard calculation on the NACA 0012 rotor at an advance ratio, μ, of 0.45.

correspondingly less sensitive to manipulation of the starting conditions. Separation on the rotor is affected little by three-dimensionality; the predicted separation positions given by the "standard" calculations and by the "two-dimensional" calculations, at this condition, are indistinguishable. Starting the calculation further downstream is more effective in delaying separation (as was noted under "Presentation of Results," above), because the region of high gradients is thereby avoided altogether. This latter is, of course, no answer to the problem of early separation because, in the real flow, the turbulent boundary layer is virtually forced to start close to the suction peak* unless a laminar bubble is present at the leading edge (see "Pessimistic Separation Predictions," above).

Because of this difference in behavior, the two-dimensional airfoil was not a particularly good model of conditions over the forward part of the rotor. However, the important conclusion which can be drawn from this study is that the early separation predicted for the rotor cannot easily be attributed to inadequacies in the assumed starting conditions. Indeed, in the light of these calculations it seems more and more likely that the effects of time-dependence, which have been neglected in the present work, is the controlling factor for rotor separation.

CONCLUSIONS

1. Some calculations of the turbulent boundary layer on a helicopter rotor have been made, which took into account crossflows and crossflow derivatives, and also centrifugal and Coriolis forces, but which neglected the effects of time-dependence; the blade was assumed to be "frozen" at any given azimuthal position. The pressure distribution on the blade was found from two-dimensional, potential-flow strip theory, using empirical data for the variation of local angle of incidence. Results were obtained covering a range of rotor conditions, and relating to two different blade sections: an NACA 0012 section and an "advanced" airfoil section.

2. A study was made of the effects of neglecting either spanwise derivatives or spanwise velocities and derivatives in the boundary layer equations. Neglect of the spanwise derivatives corresponds (approximately) to the assumption that the boundary layer behaves like that on an infinite yawed wing. Under the conditions considered, it was found that this had little effect on the calculations, no doubt as a result of the high aspect ratio of the blades. Neglect of spanwise velocities and derivatives corresponds to the assumption that the boundary layer behaves like a two-dimensional one. There were noticeable differences between the results of these latter calculations and the results of the fully three-dimensional calculations.

3. Early separation of the turbulent boundary layer was predicted over almost one-half of the blade disc. In contrast, wind-tunnel and flight tests indicate rotor stall over a considerably smaller range of conditions. Because of this measure of disagreement, it was decided not to present the results of the calculations as a set of reference data. Instead, some effort was made to determine the cause of the pessimistic separation predictions. A number of factors were identified which might have contributed, ranging

---

*At the suction peak, the value of $(c/u_e)(\partial u_e/\partial x)$ is zero.

from inadequacies in the theoretical pressure distributions to inadequacies in the starting conditions for the turbulent boundary layer. However, with the exception of the effects of time-dependence, which could not be examined with the existing calculation method, none of these factors appeared to be serious enough to account for a large error in predicted separation position.

4. The discrepancy between the calculated and the observed stall boundaries probably cannot be resolved until the effects of time-dependence can be taken into account in the calculations. Therefore, there is a strong incentive to proceed to a further study of rotor boundary layers in which these effects are included.

AIRFOIL
SECTION
SHAPE

VARIATION OF
EFFECTIVE BLADE
INCIDENCE

POTENTIAL-FLOW
CALCULATION

PRESSURE
DISTRIBUTION

BOUNDARY-
LAYER
CALCULATION

BOUNDARY-
LAYER
CHARACTERISTICS

COMPARISON
WITH STRIP
THEORY

[COMPARISON
WITH
EXPERIMENT]
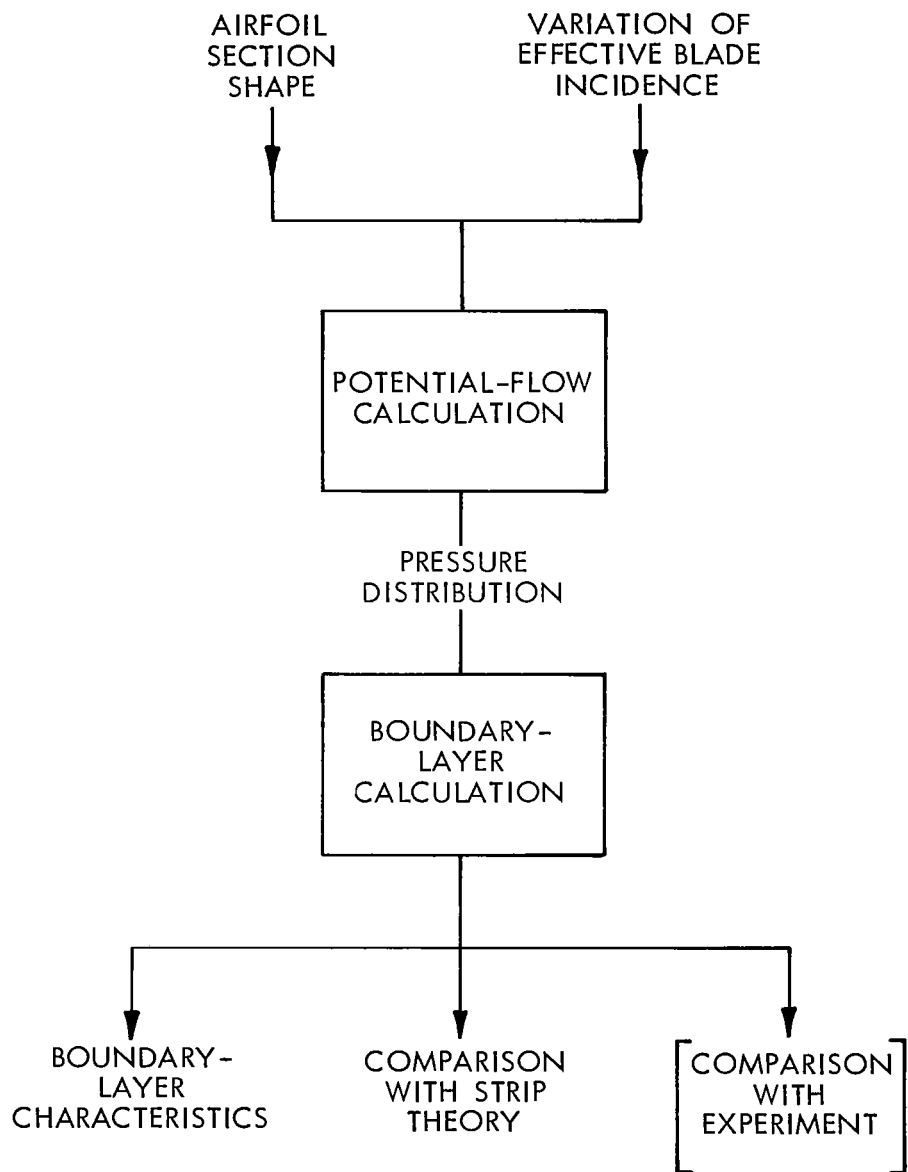
FIGURE 1. THE CALCULATION METHOD.
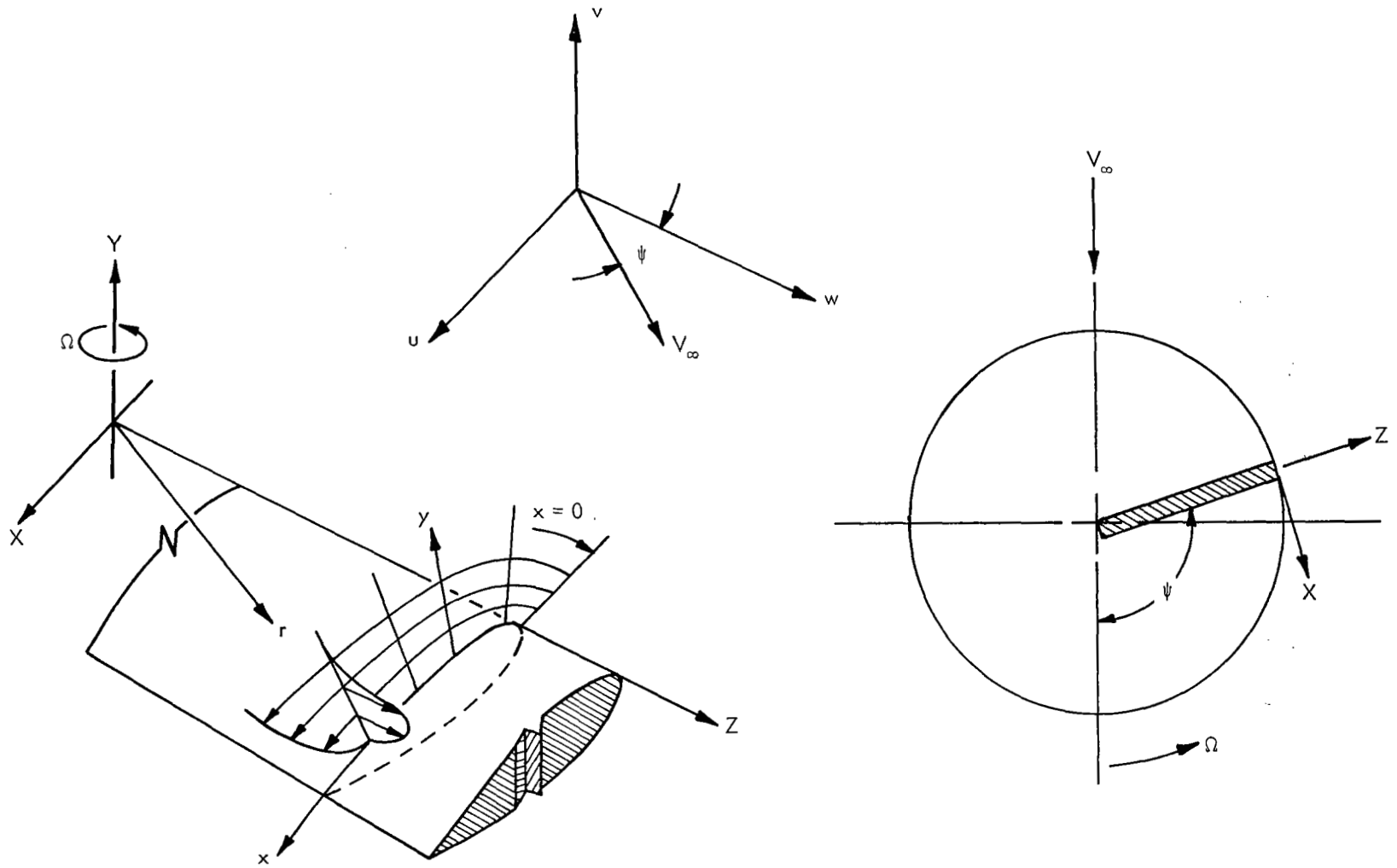
FIGURE 2. – COORDINATES IN THE ROTATING SYSTEM
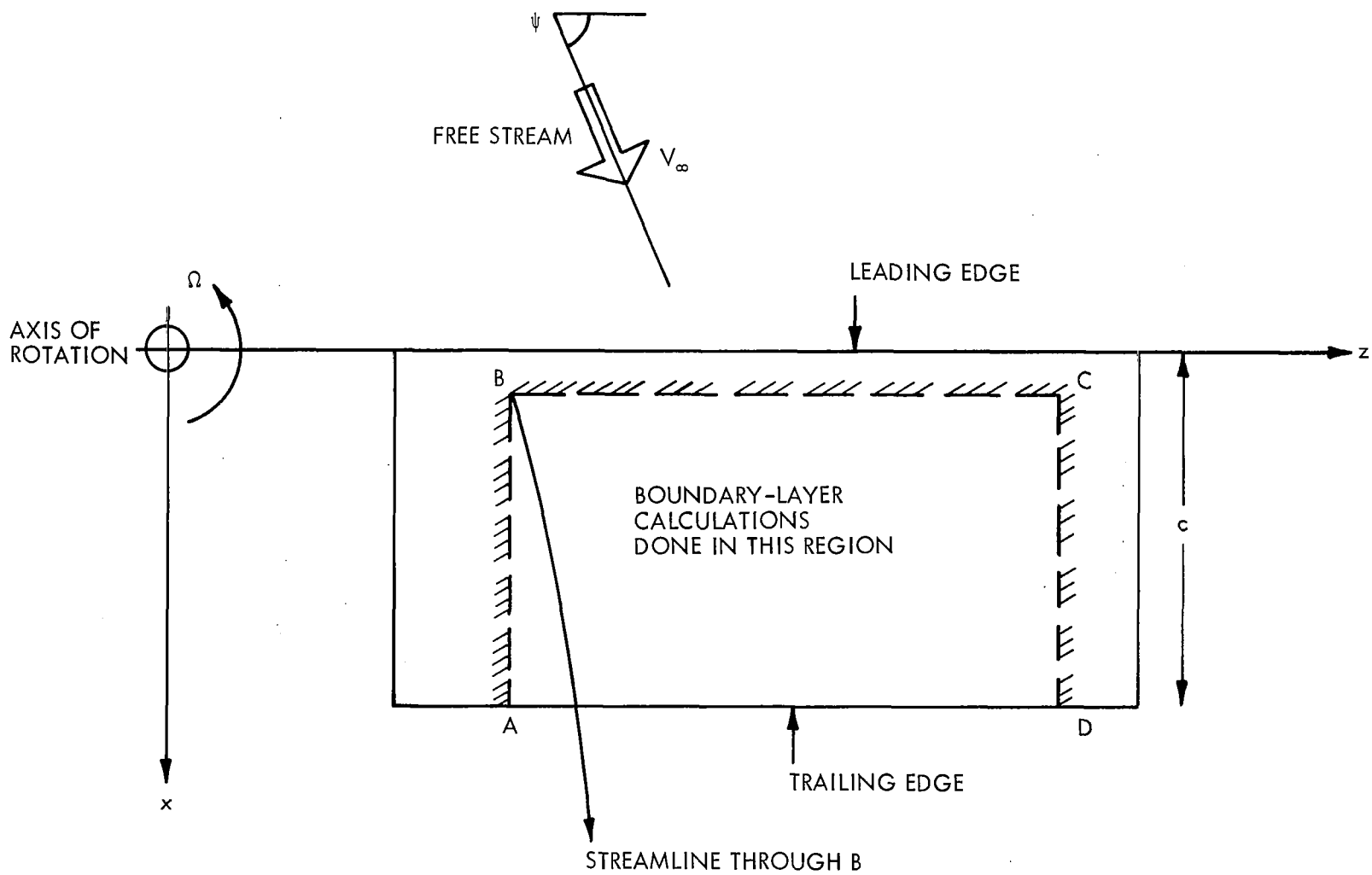
FIGURE 3. - SCHEMATIC DIAGRAM OF ROTOR BLADE
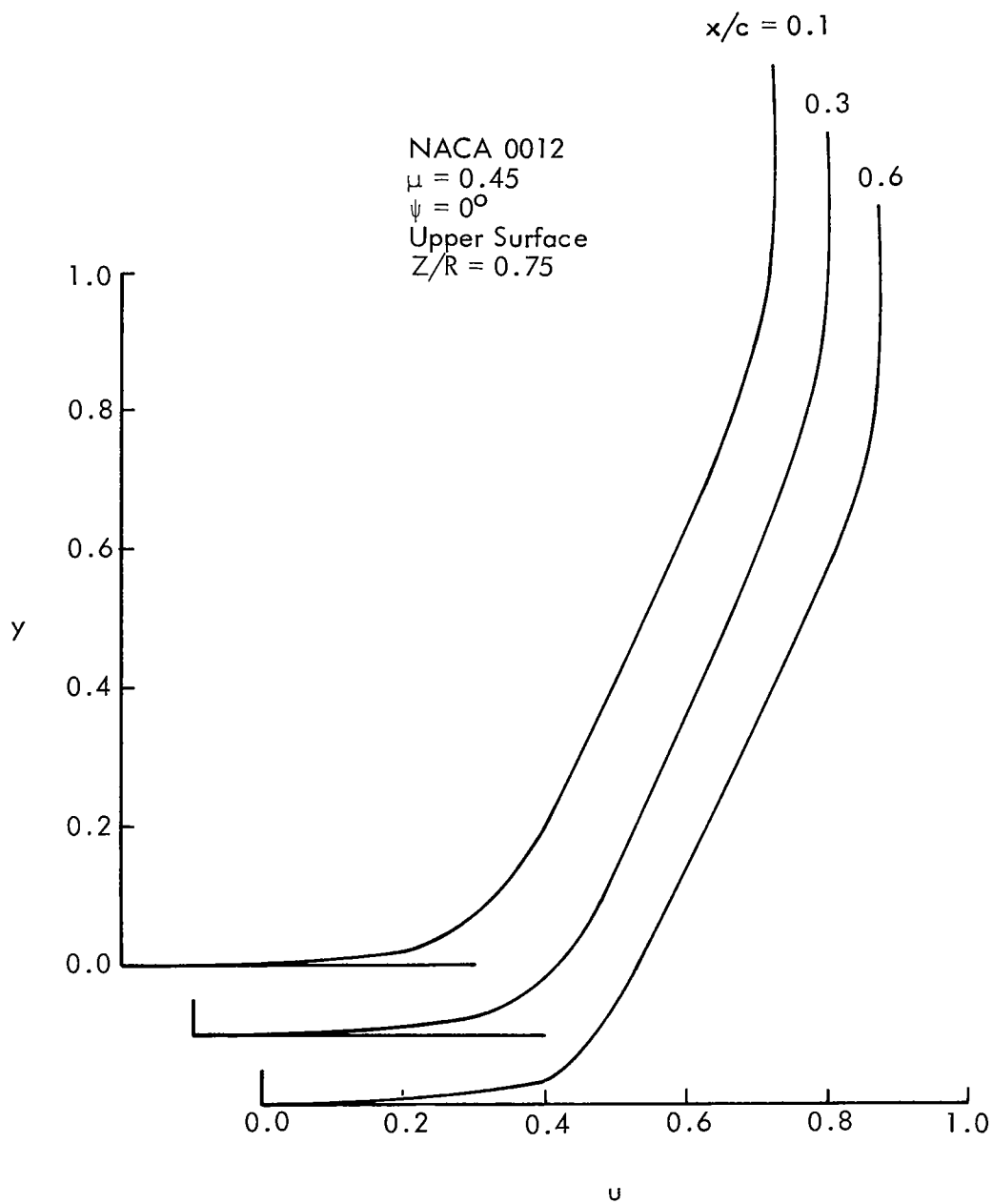
FIGURE 4. CHORDWISE VELOCITY PROFILES.

NACA 0012
$\mu = 0.45$
$\psi = 0°$
LOWER SURFACE
$z/R = 0.75$

x/c = 0.1

0.3

0.6

0.9
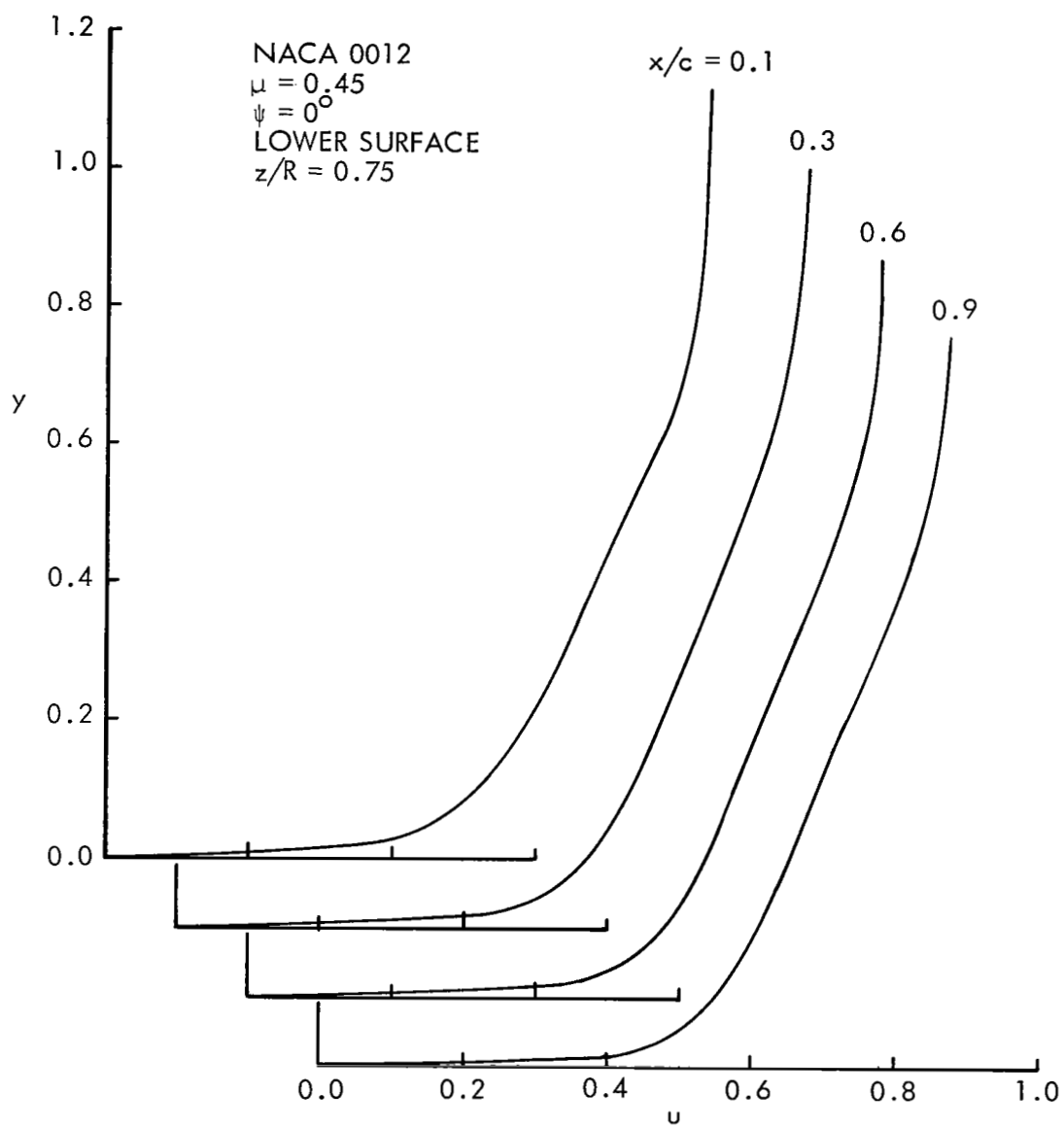
FIGURE 4. (CONTINUED)

FIGURE 4. (CONTINUED)

ADVANCED AIRFOIL
$\mu = 0.23$
$\psi = 0^{\circ}$
Upper Surface
$Z/R = 0.75$

FIGURE 4. (CONTINUED)

YAWED WING
$\mu = 0.45$
$\psi = 0°$
Upper Surface
$Z/R = 0.75$

$x/c = 0.1$
0.3
0.6

FIGURE 4. (CONTINUED)

24

TWO-DIMENSIONAL CASE
$\mu = 0.45$
$\psi = 0°$
Upper Surface
$Z/R = 0.75$
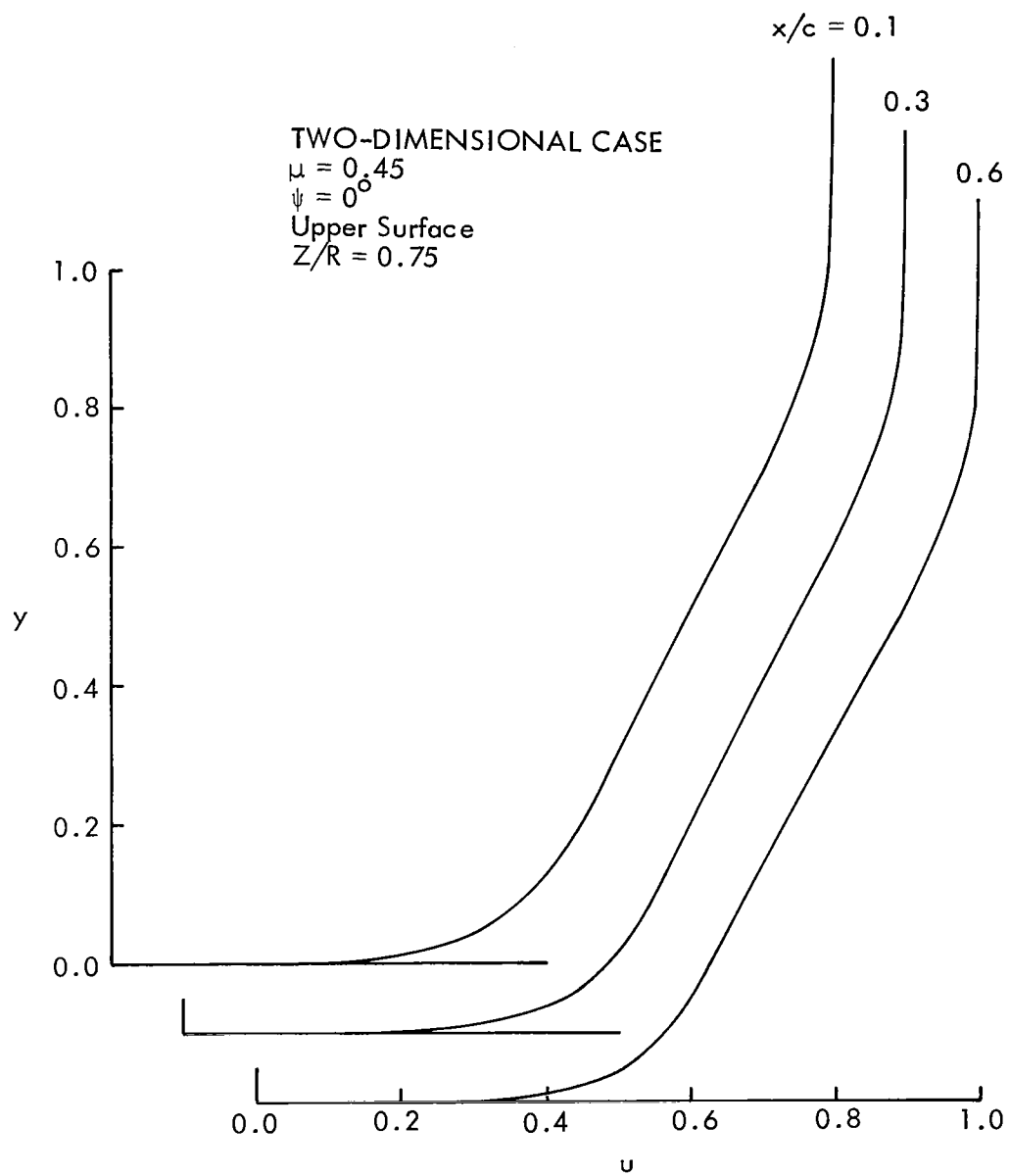
FIGURE 4. (CONTINUED)

NACA 0012
$\mu = 0.45$
$\psi = 0°$
Upper Surface
$Z/R = 0.75$

x/c = 0.1
0.3
0.6
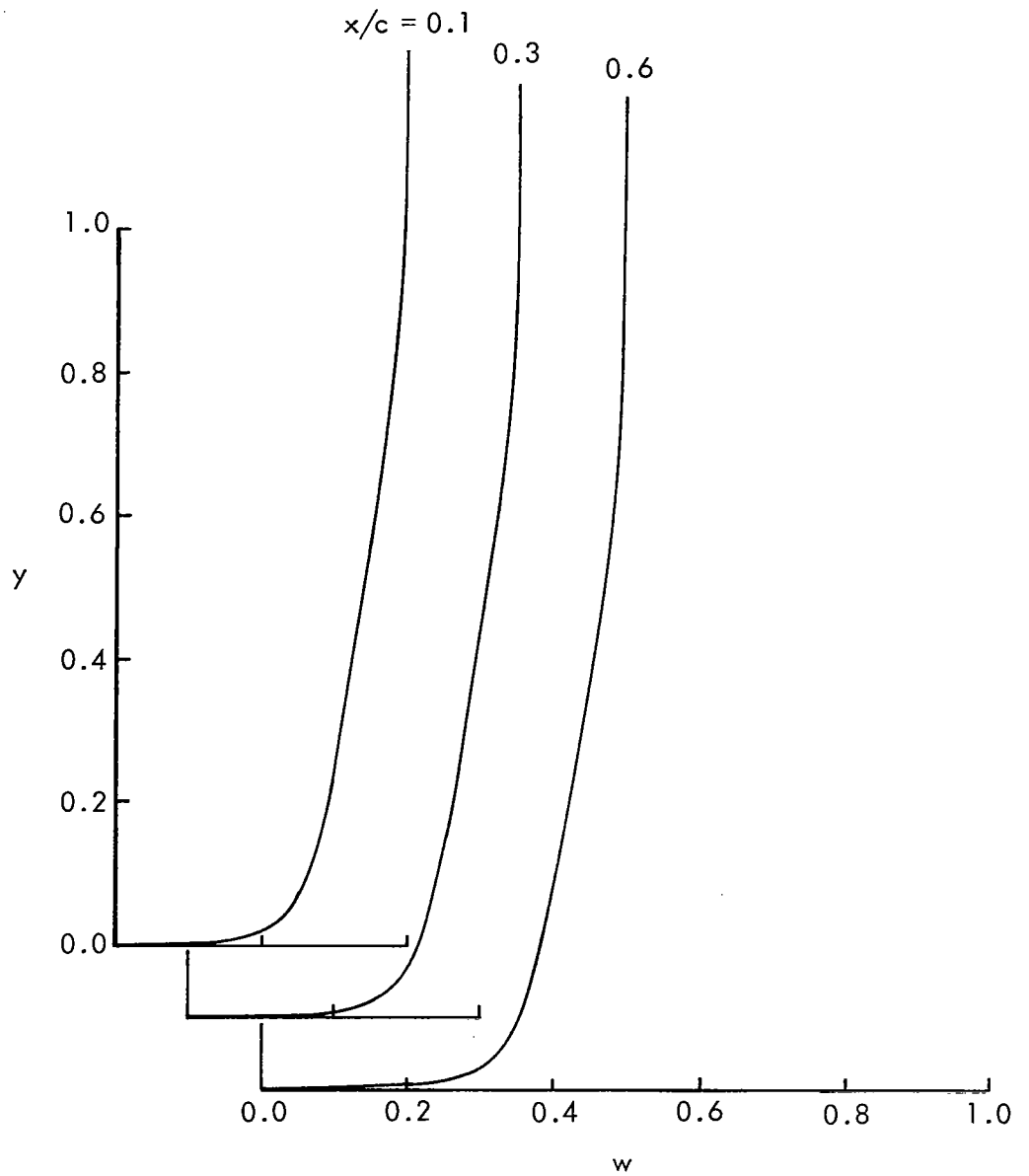
FIGURE 5. SPANWISE VELOCITY PROFILES.
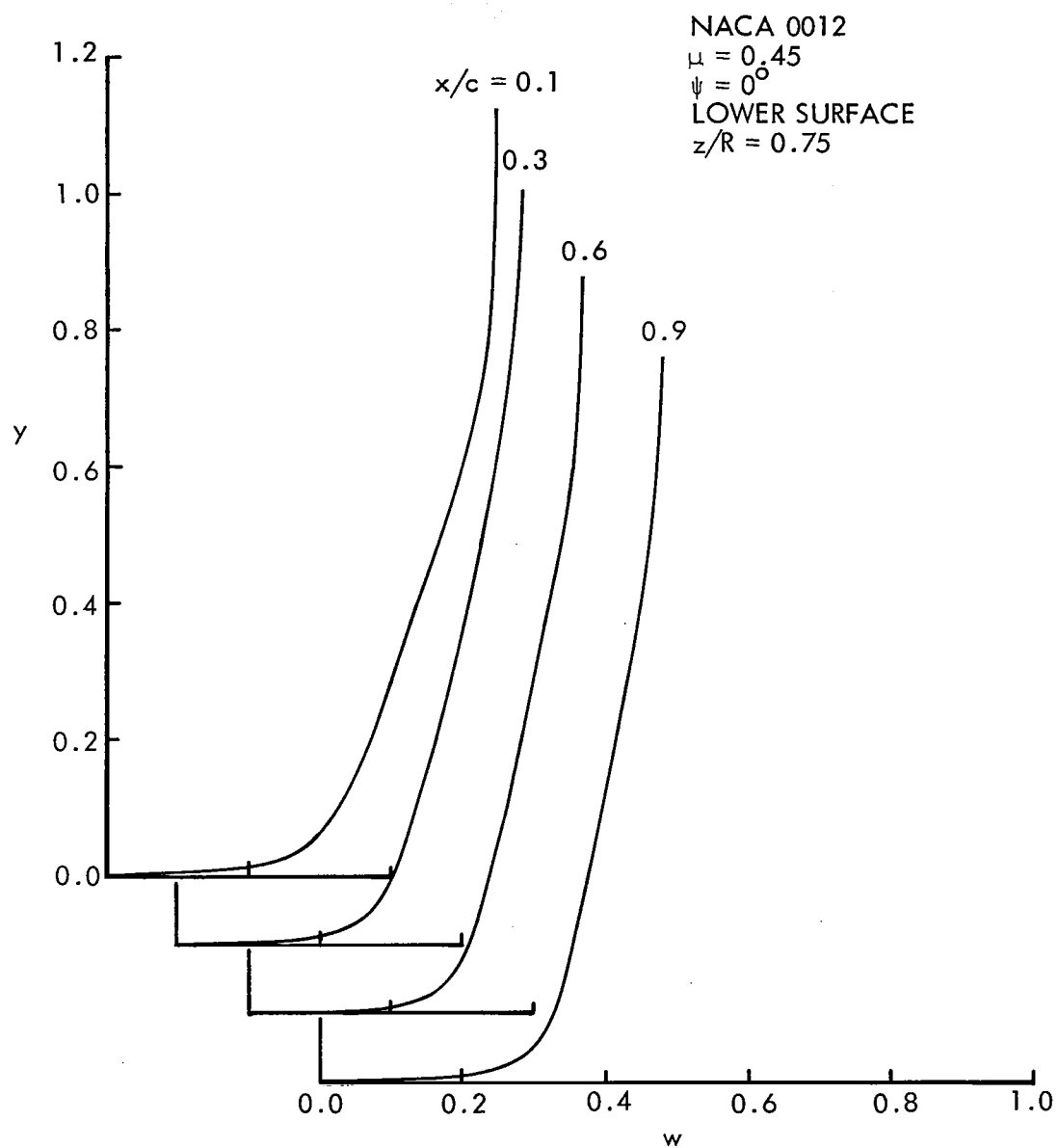
FIGURE 5. (CONTINUED)

NACA 0012
$\mu = 0.23$
$\psi = 0^\circ$
Upper Surface
$Z/R = 0.75$
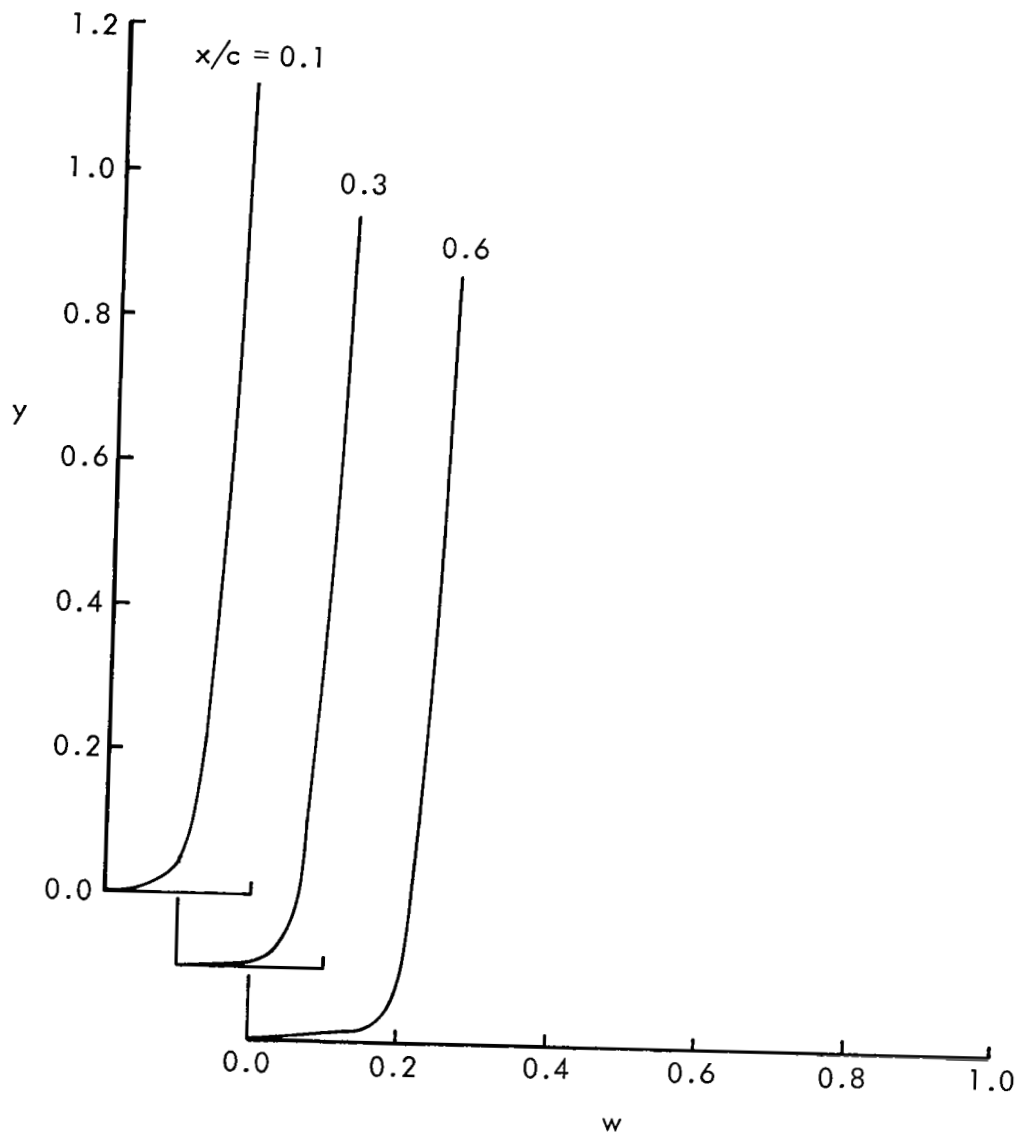
FIGURE 5. (CONTINUED)

ADVANCED AIRFOIL
$\mu = 0.23$
$\psi = 0^{\circ}$
Upper Surface
$Z/R = 0.75$
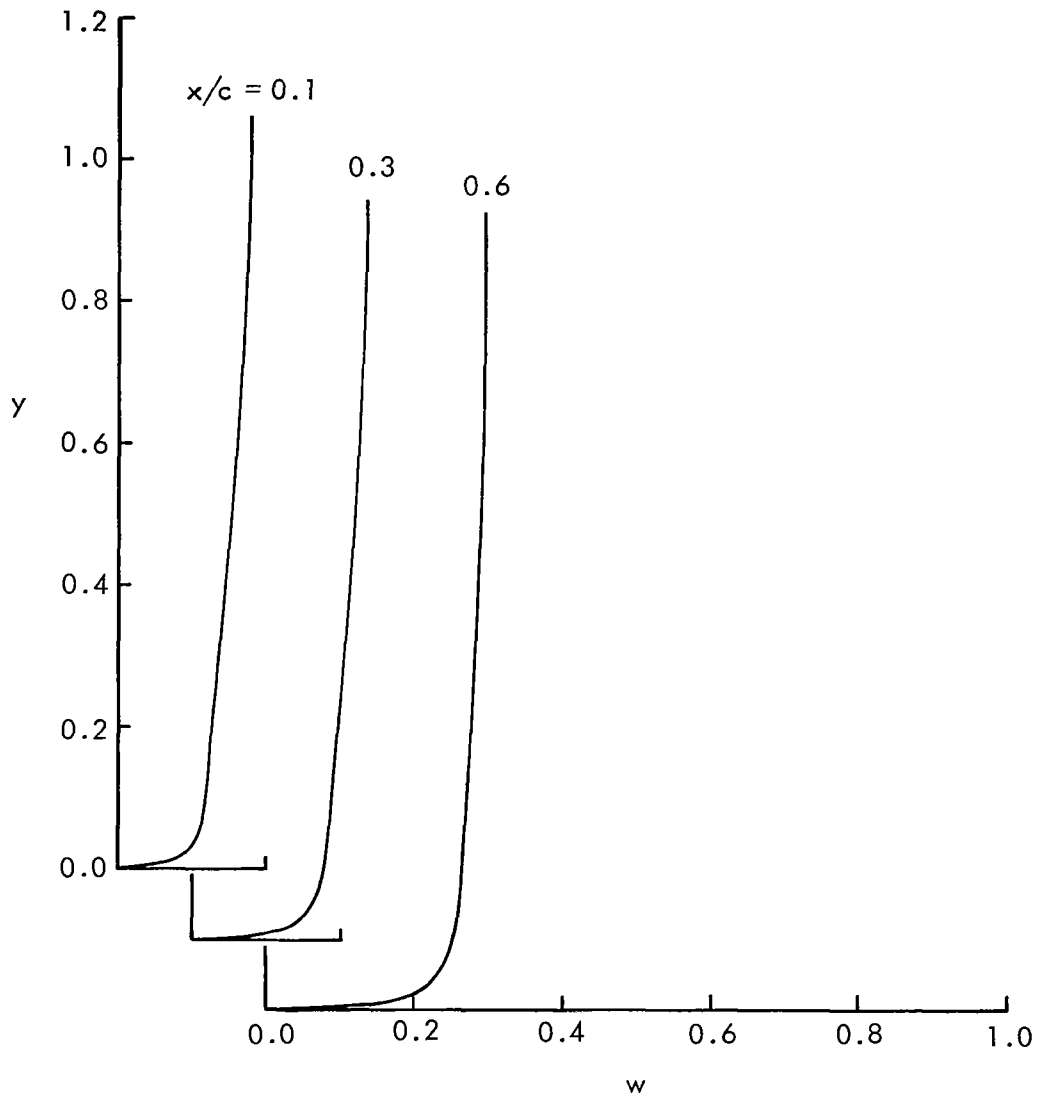
FIGURE 5. (CONTINUED)

YAWED WING
$\mu = 0.45$
$\psi = 0°$
Upper Surface
$Z/R = 0.75$

FIGURE 5. (CONTINUED)

30
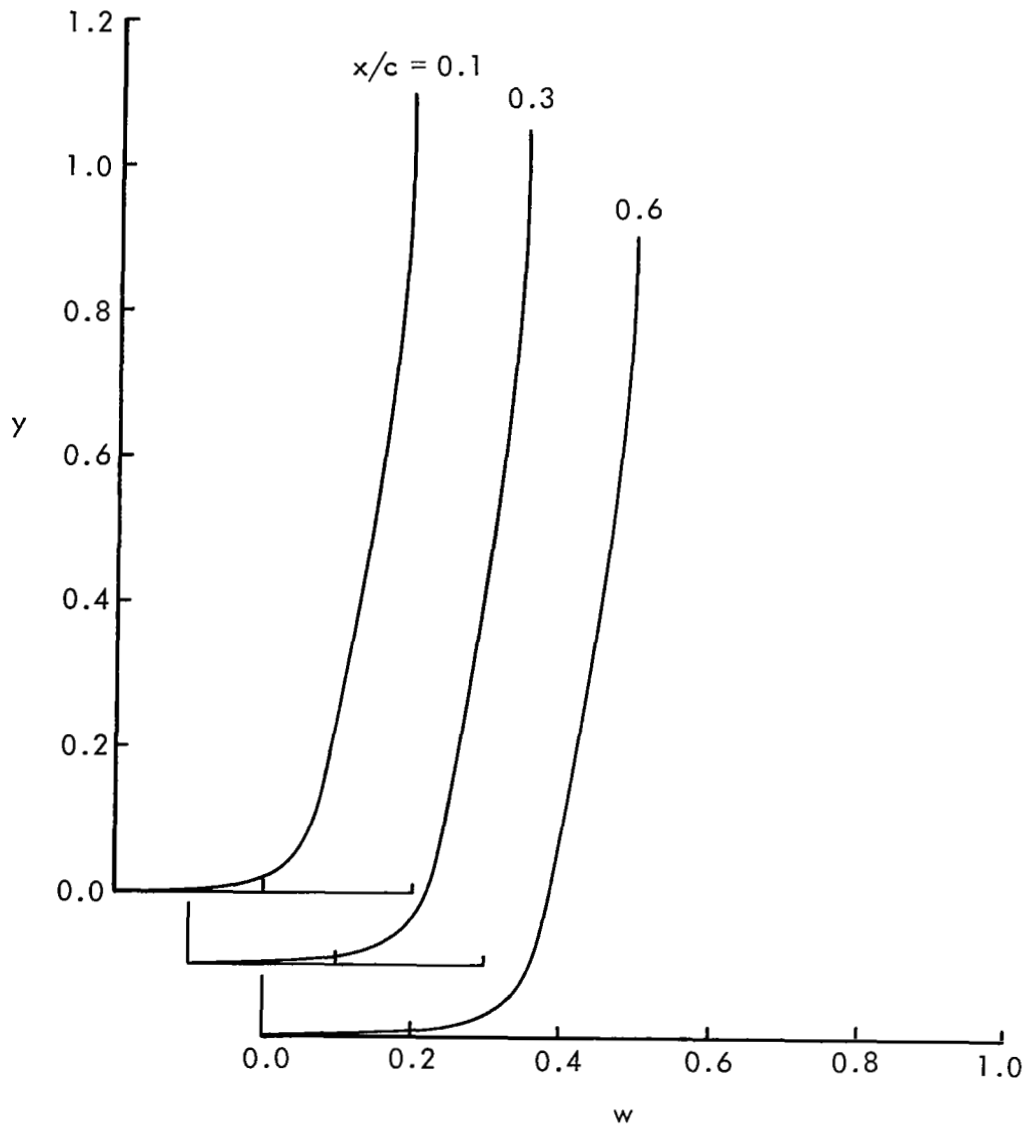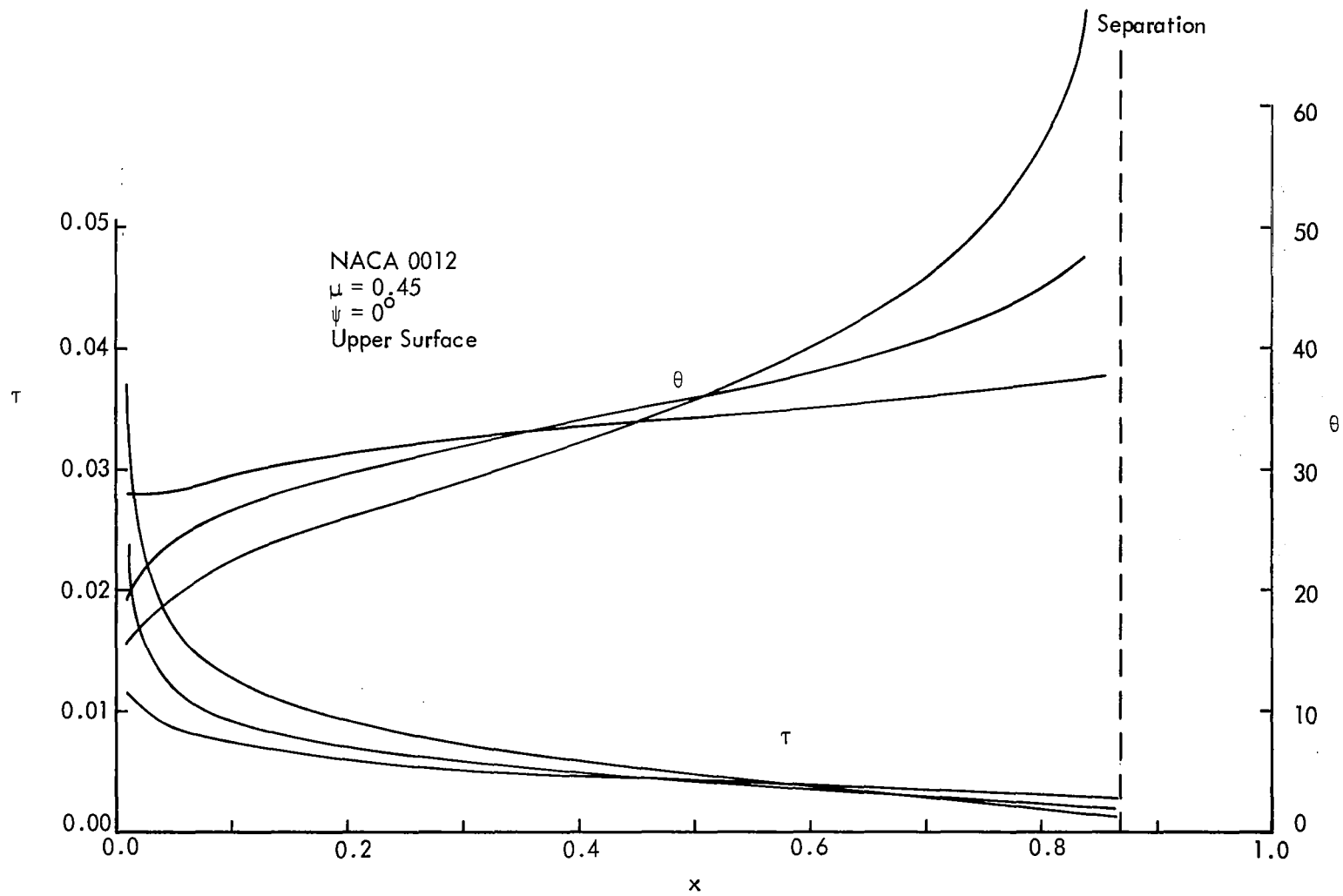
FIGURE 6. WALL SHEAR STRESS VARIATION ALONG CHORD.
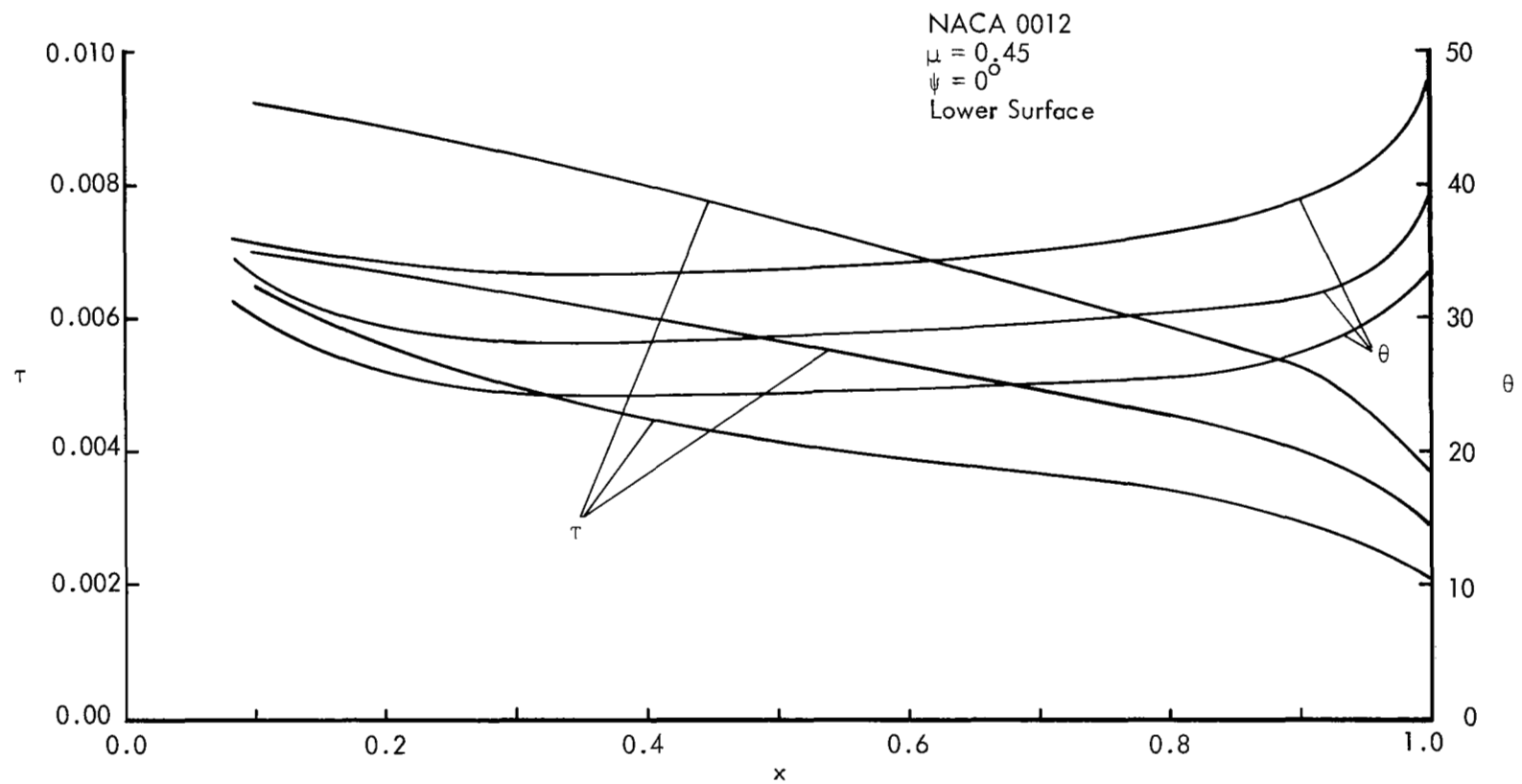
FIGURE 6. (CONTINUED)
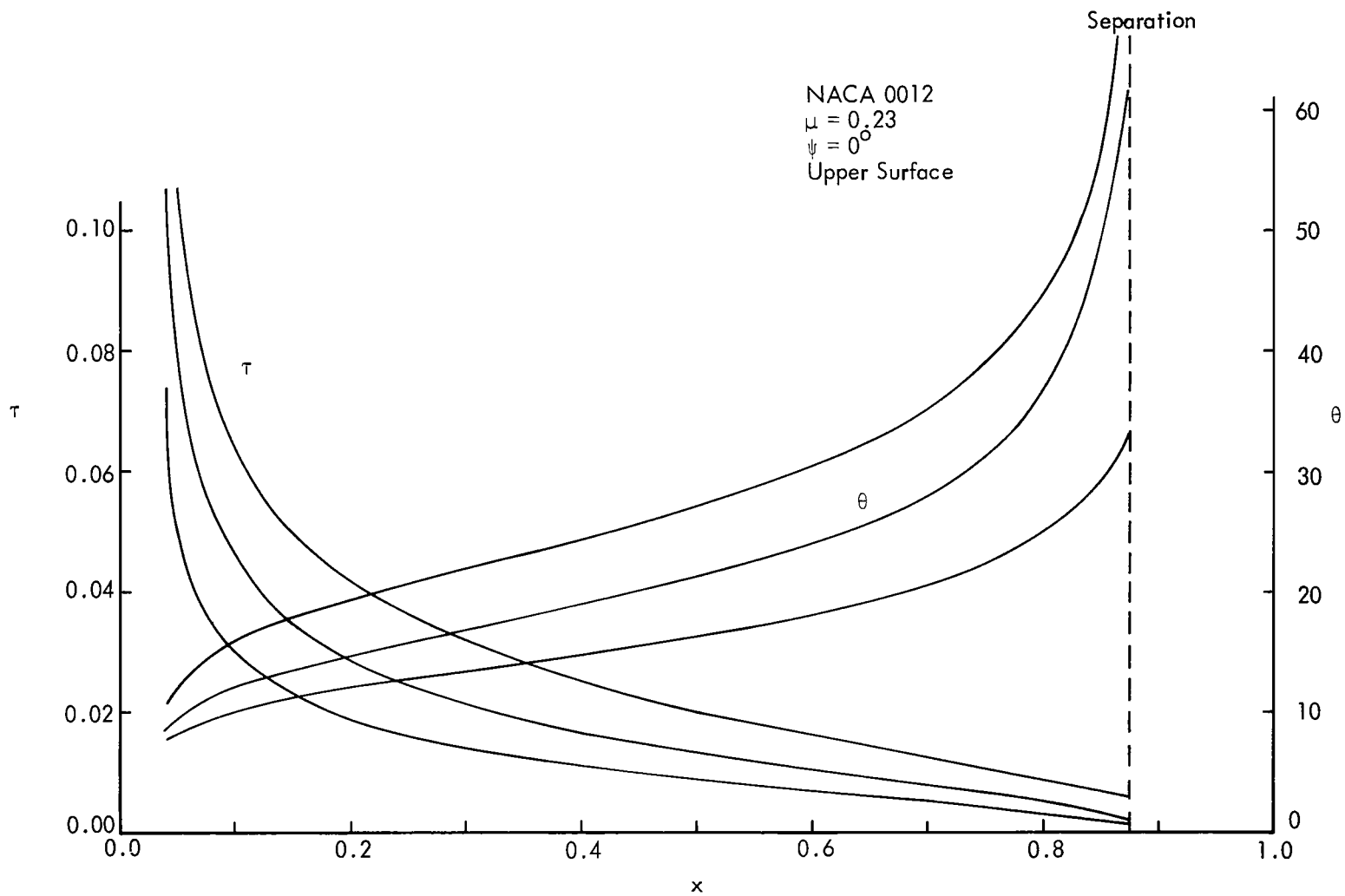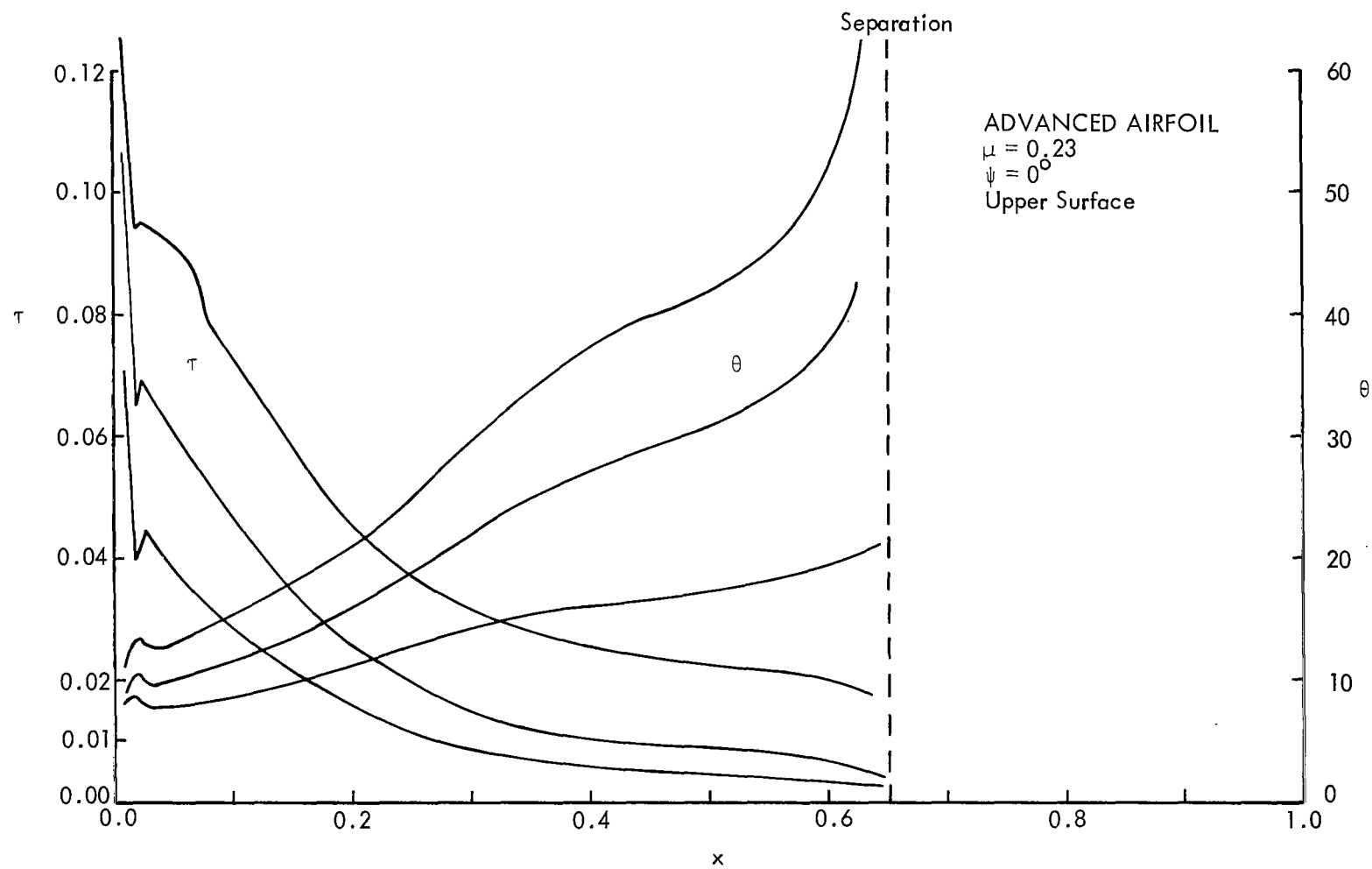
FIGURE 6. (CONTINUED)
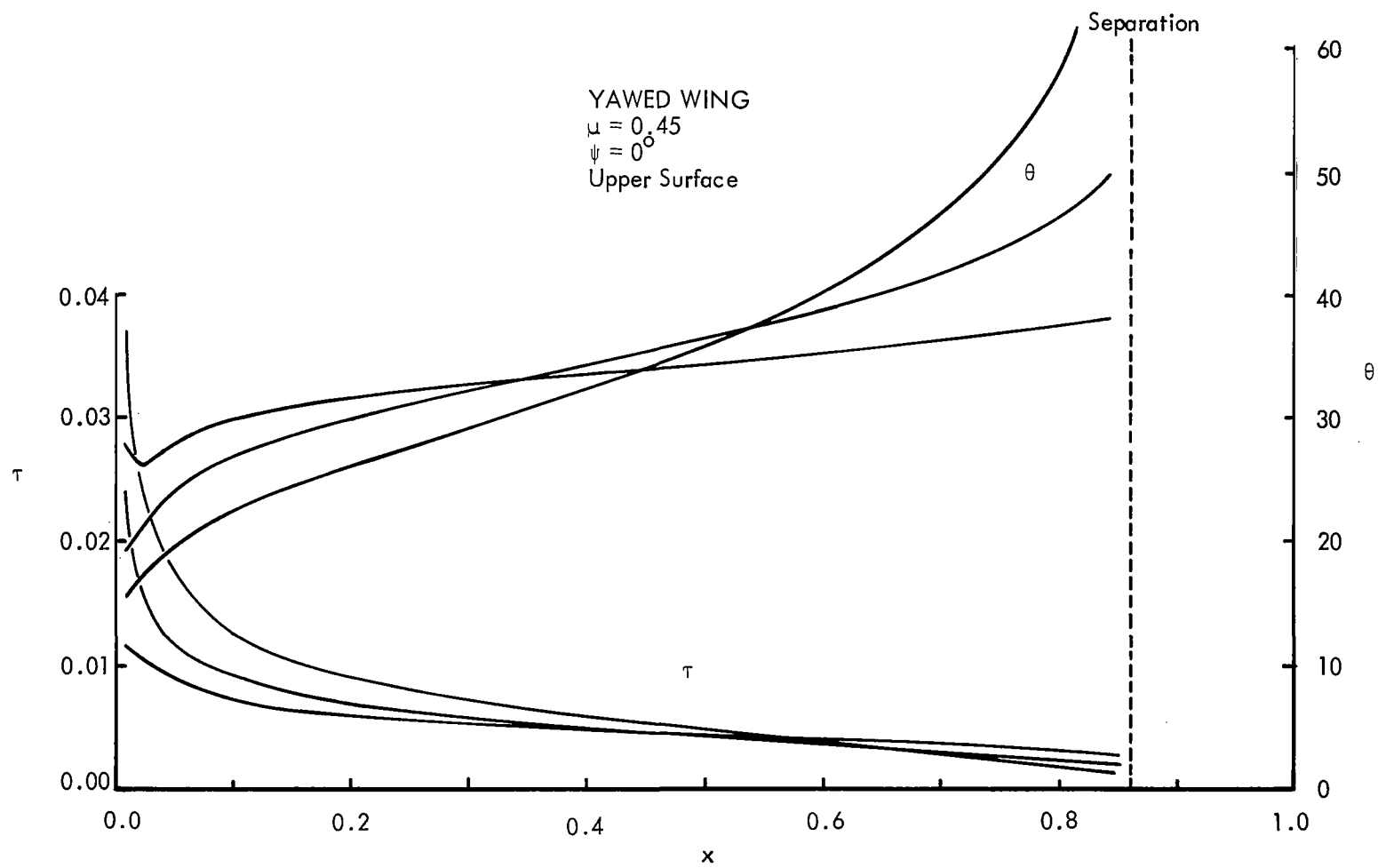
FIGURE 6. (CONTINUED)
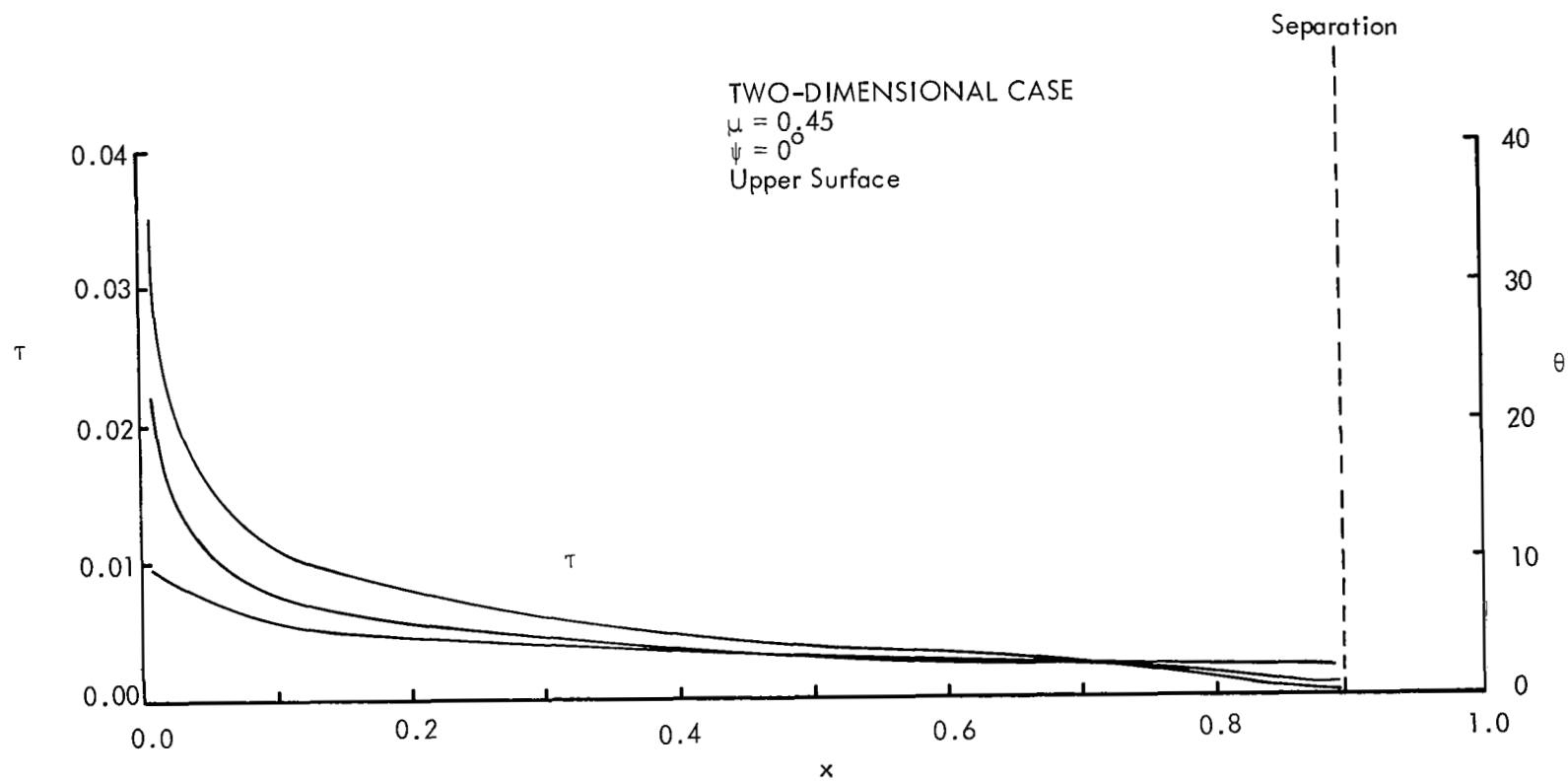
FIGURE 6. (CONTINUED)

FIGURE 6. (CONTINUED)
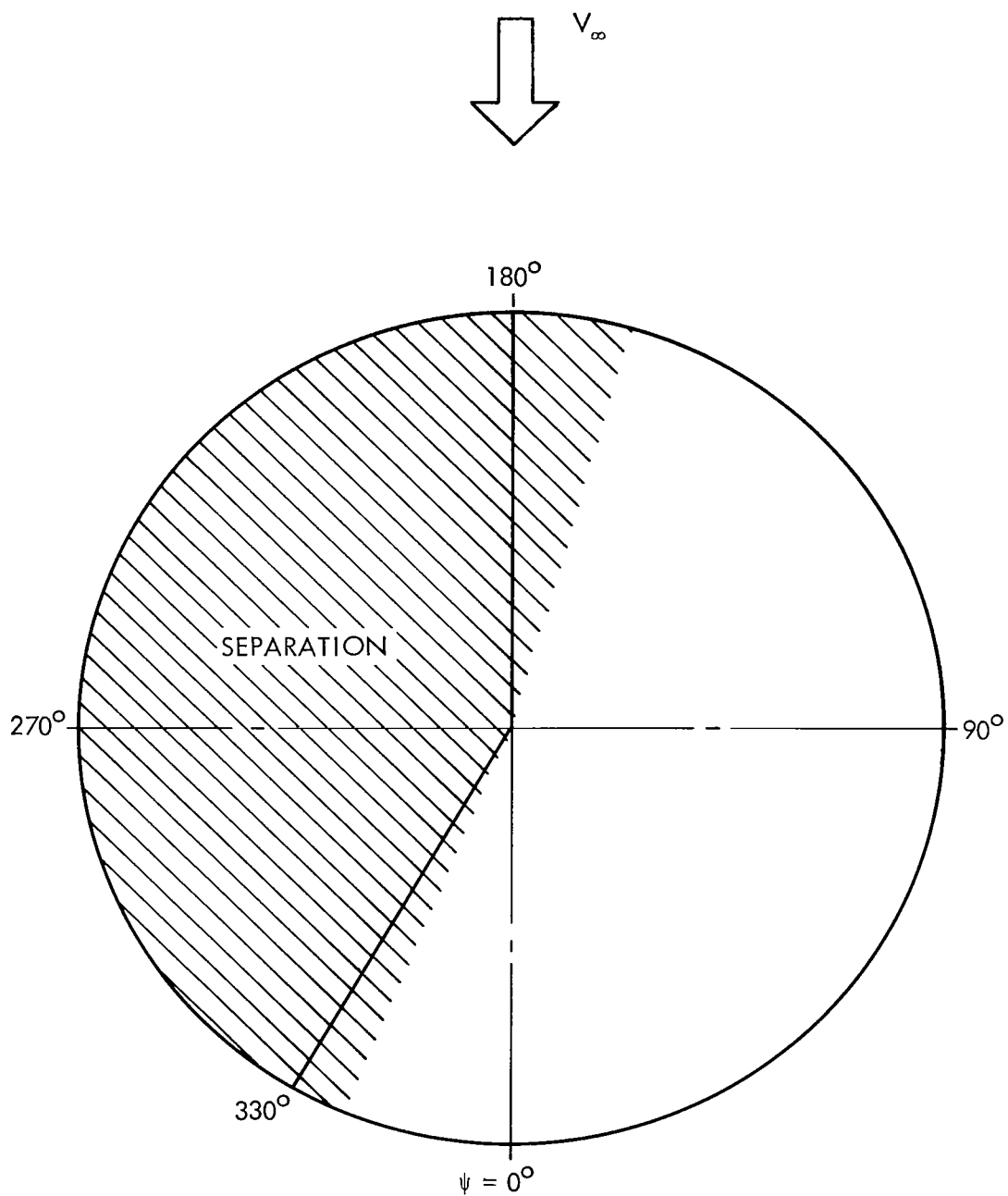
FIGURE 7. PREDICTED OCCURRENCE OF SEPARATION.
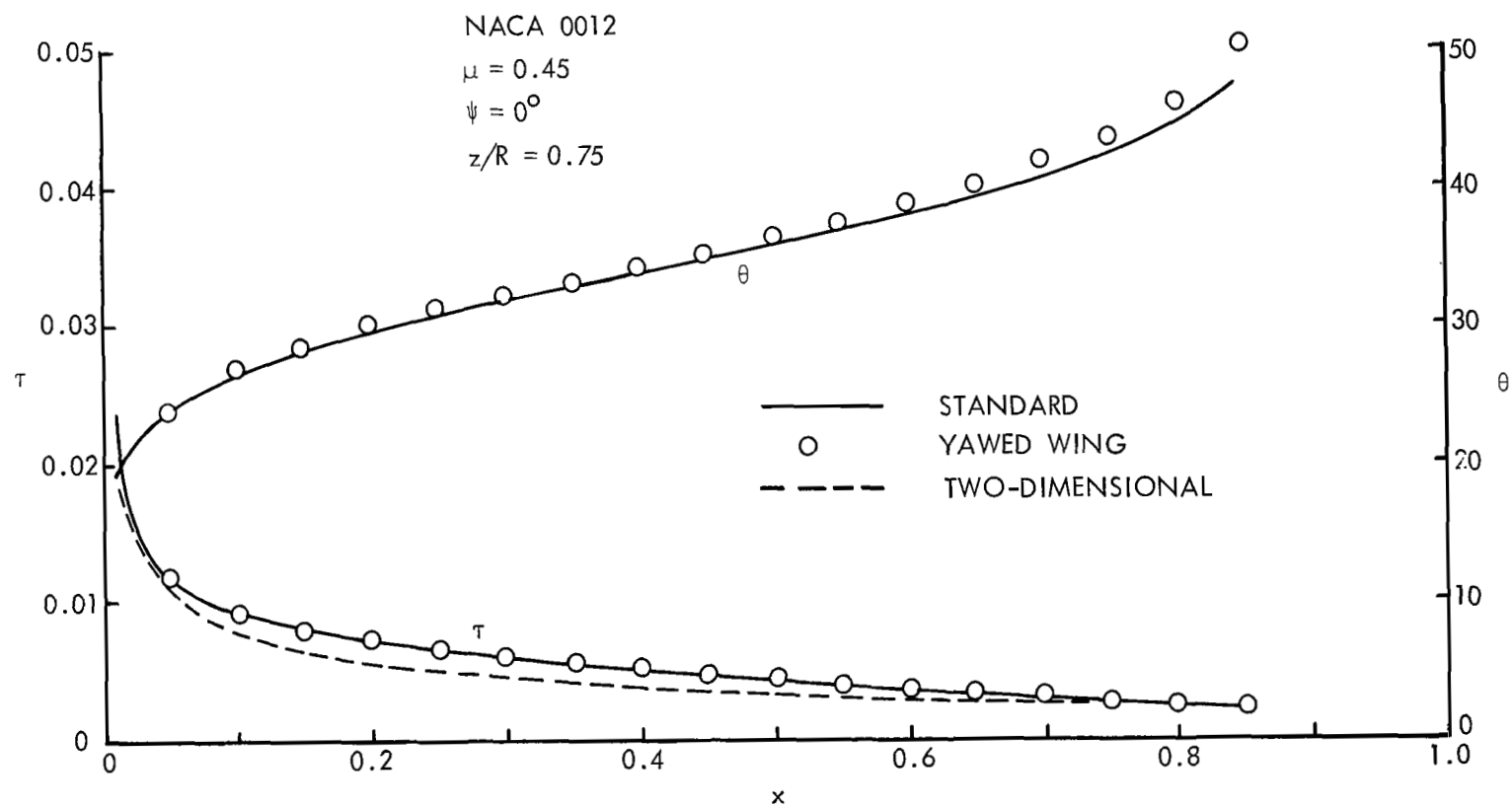
FIGURE 8. EFFECT OF THREE-DIMENSIONALITY IN THE BOUNDARY LAYER.
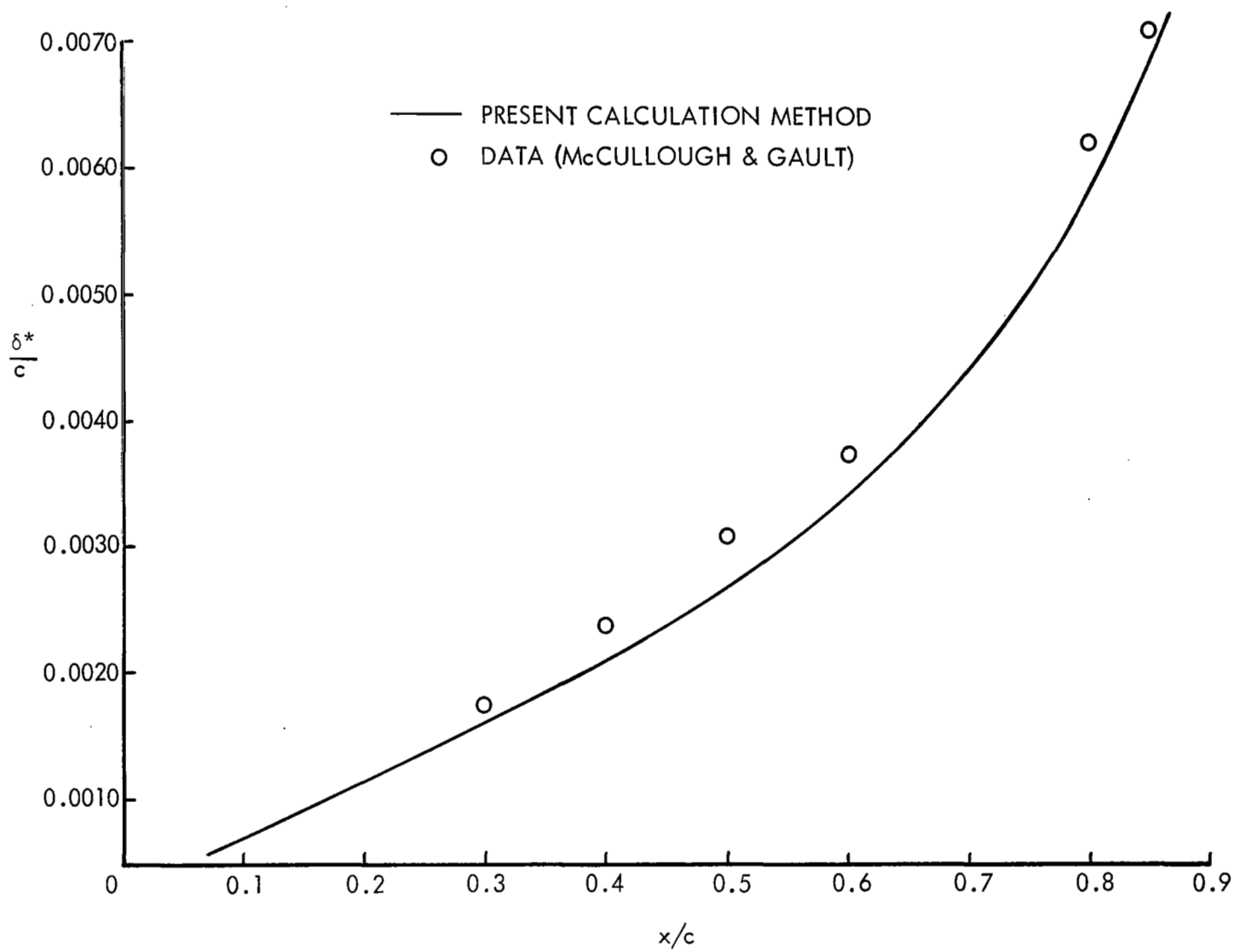
FIGURE 9   CALCULATIONS FOR A TWO-DIMENSIONAL AIRFOIL

NACA 63-009 AIRFOIL

$\alpha = 8.5^{o}$

—————— PRESENT CALCULATION

⬡ EXPERIMENTAL DATA
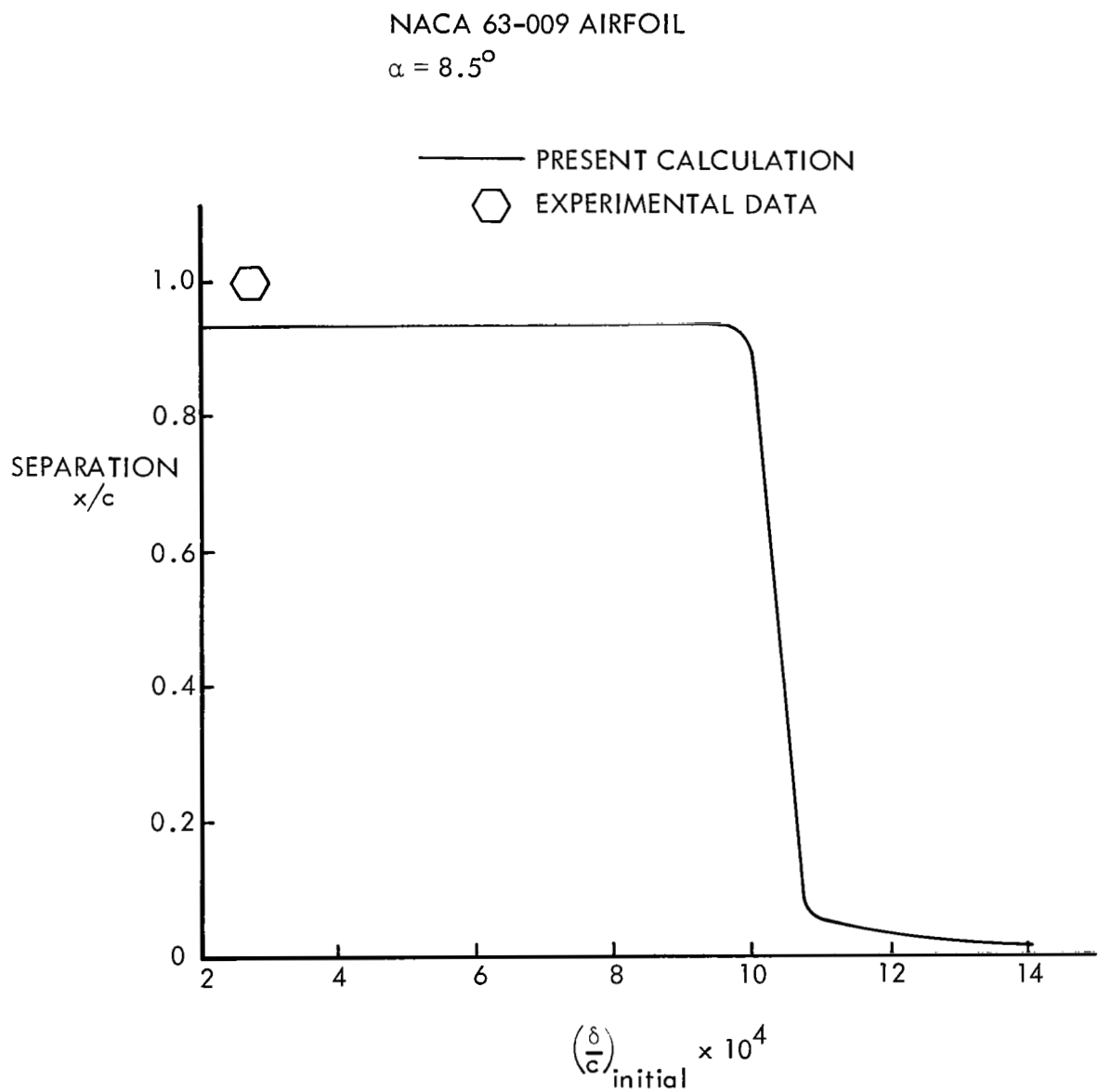
FIGURE 10   SENSITIVITY OF THE FLOW ON THE TWO-DIMENSIONAL AIRFOIL
TO VARIATION OF THE INITIAL BOUNDARY-LAYER THICKNESS
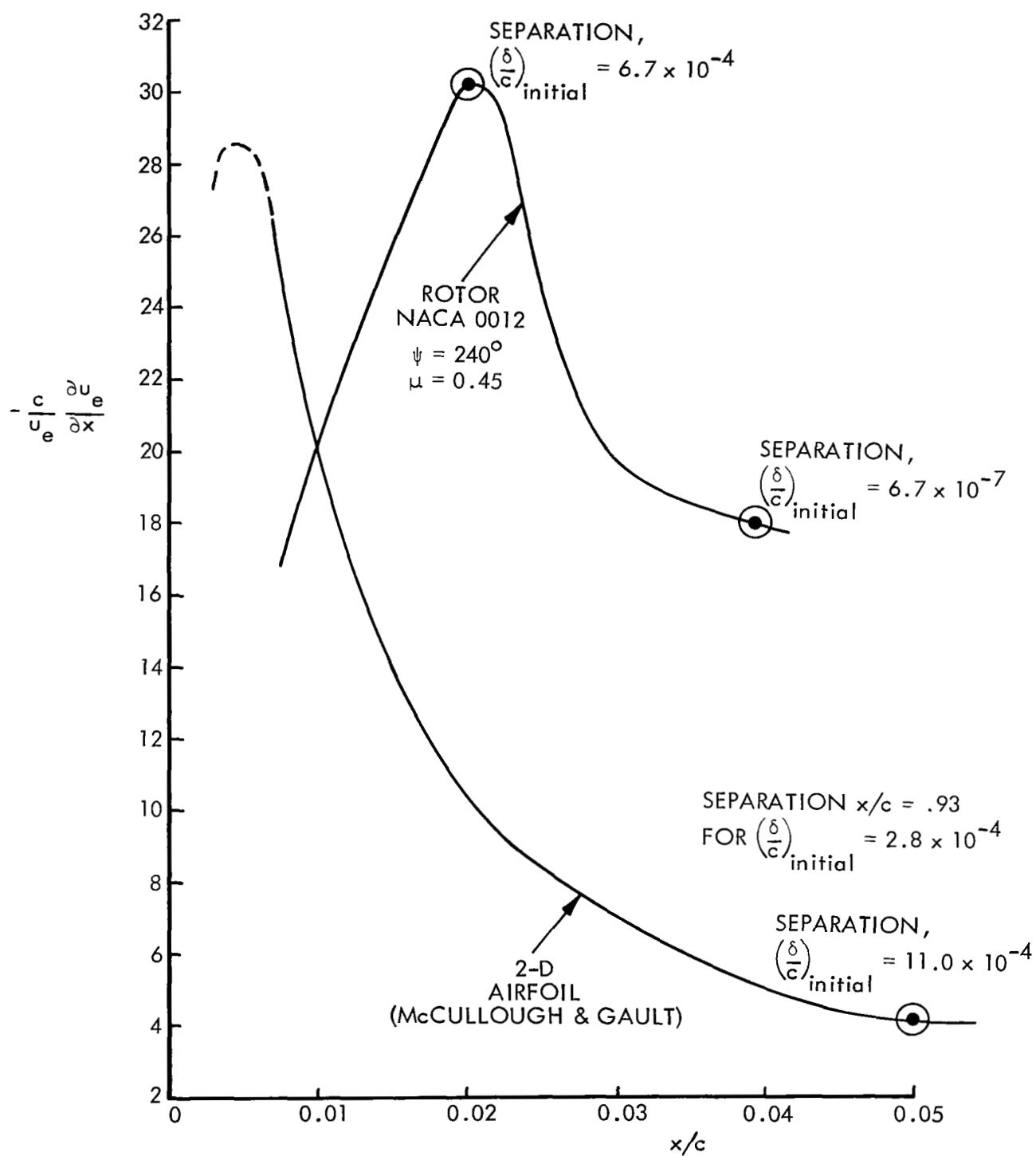
FIGURE 11   POTENTIAL–FLOW VELOCITY GRADIENT ON THE ROTOR AND ON
THE TWO–DIMENSIONAL AIRFOIL

41

TABLE I

SUMMARY OF CALCULATED RESULTS

Case	μ	ψ	Surface	z/R	x/c	u_e	w_e	δ/c	Initial x/c	Separation x/c	T
NACA 0012 (standard)	0.45	0°	Upper	0.60 $\alpha=2.73°$	0.1	1.865	0.999	0.0029	0.0096	0.868	0.0035
					0.3	1.694	0.979	0.0067			
					0.6	1.531	0.935	0.0127			
					0.9	-	-	-			
				0.75 $\alpha=4.62°$	0.1	2.339	0.999	0.0030	0.0096	0.868	0.0040
					0.3	1.967	0.978	0.0078			
					0.6	1.656	0.931	0.0161			
					0.9	-	-	-			
				0.90 $\alpha=5.06°$	0.1	2.883	0.997	0.0029	0.0096	0.868	0.0051
					0.3	2.359	0.987	0.0080			
					0.6	1.906	0.964	0.0179			
					0.9	-	-	-			
NASA 0012 (standard)	0.45	0°	Lower	0.60 $\alpha=2.73°$	0.1	1.373	0.988	0.0011	0.0843	No	0.0031
					0.3	1.458	0.958	0.0046			
					0.6	1.406	0.922	0.0094			
					0.9	1.300	0.888	0.0152			
				0.75 $\alpha=4.62°$	0.1	1.509	0.988	0.0010	0.0843	No	0.0044
					0.3	1.732	0.958	0.0040			
					0.6	1.714	0.922	0.0084			
					0.9	1.609	0.887	0.0136			
				0.90 $\alpha=5.06°$	0.1	1.788	0.989	0.0009	0.0843	No	0.0059
					0.3	2.051	0.966	0.0037			
					0.6	2.039	0.934	0.0078			
					0.9	1.912	0.900	0.0127			

TABLE I. — Continued

SUMMARY OF CALCULATED RESULTS

Case	μ	ψ	Surface	z/R	x/c	u_e	w_e	δ/c	Initial x/c	Separation x/c	T
NACA 0012 (standard)	0.23	0°	Upper	0.60	0.1	4.316	0.992	(0.0021)	0.0096	0.051	0.0013
				$\alpha=8.89°$	0.3	3.369	0.972	(0.0076)	(0.0381)	0.878	0.0101
					0.6	2.710	0.920	(0.177)			
					0.9	-	-	-			
				0.75	0.1	5.438	0.986	(0.0021)	0.0096	0.051	0.0023
				$\alpha=8.67°$	0.3	4.250	0.961	(0.0071)	(0.0381)	0.878	0.0158
					0.6	3.414	0.912	(0.168)			
					0.9	-	-	-			
				0.90	0.1	6.370	0.981	(0.0018)	0.0096	0.051	0.0033
				$\alpha=7.28°$	0.3	5.117	0.952	(0.0064)	(0.0381)	0.878	0.0232
					0.6	4.188	0.904	(0.0147)			
					0.9	-	-	-			
Advanced Airfoil	0.23	0°	Upper	0.60	0.1	4.225	0.995	0.0030	0.0096	0.652	0.0078
				$\alpha=8.89°$	0.3	3.121	0.973	0.0097	(0.1)	No	0.0114
					0.6	2.382	0.913	0.0267			
					0.9	-	-	-			
				0.75	0.1	5.420	0.992	0.0027	0.0096	0.652	0.0135
				$\alpha=8.67°$	0.3	4.067	0.987	0.0087	(0.1)	No	0.0173
					0.6	3.157	0.970	0.0226			
					0.9	-	-	-			
				0.90	0.1	6.751	0.988	0.0022	0.0096	0.652	0.0248
				$\alpha=7.28°$	0.3	5.394	0.993	0.0069	(0.1)	No	0.0243
					0.6	4.489	1.003	0.0156			
					0.9	-	-	-			

TABLE I. — Continued

SUMMARY OF CALCULATED RESULTS

Case	μ	ψ	Surface	z/R	x/c	u_e	w_e	δ/c	Initial x/c	Separation x/c	T
NACA 0012 (yawed wing)	0.45	0°	Upper	0.60 $\alpha=2.73^\circ$	0.1 0.3 0.6 0.9	1.865 1.694 1.531 -	0.999 0.979 0.935 -	0.0028 0.0068 0.0129 -	0.0096	0.863	0.0035
				0.75 $\alpha=4.62^\circ$	0.1 0.3 0.6 0.9	2.337 1.965 1.654 -	0.999 0.978 0.931 -	0.0030 0.0078 0.0163 -	0.0096	0.863	0.0039
				0.90 $\alpha=5.06^\circ$	0.1 0.3 0.6 0.9	2.880 2.356 1.902 -	0.997 0.987 0.964 -	0.0029 0.0079 0.0177 -	0.0096	0.863	0.0050
NACA 0012 (yawed wing)	0.45	0°	Lower	0.60 $\alpha=2.73^\circ$	0.1 0.3 0.6 0.9	1.373 1.458 1.406 1.301	0.988 0.958 0.922 0.888	0.0011 0.0047 0.0095 0.0155	0.084	No	0.0031
				0.75 $\alpha=4.62^\circ$	0.1 0.3 0.6 0.9	1.509 1.732 1.715 1.610	0.988 0.958 0.922 0.887	0.0010 0.0041 0.0083 0.0134	0.084	No	0.0044
				0.90 $\alpha=5.06^\circ$	0.1 0.3 0.6 0.9	1.738 2.052 2.039 1.914	0.989 0.966 0.934 0.900	0.0009 0.0038 0.0079 0.0128	0.084	No	0.0059

TABLE I. — Continued

SUMMARY OF CALCULATED RESULTS

Case	μ	ψ	Surface	z/R	x/c	u_e	w_e	δ/c	Initial x/c	Separation x/c	T
NACA 0012 (2-D)	0.45	0°	Upper	0.60 $\alpha=2.73°$	0.1	1.867	0.0	0.0026	0.0096	0.897	0.0034
					0.3	1.712	0.0	0.0062			
					0.6	1.566	0.0	0.0116			
					0.9	-	-	-			
				0.75 $\alpha=4.62°$	0.1	2.338	0.0	0.0029	0.0096	0.897	0.0038
					0.3	1.978	0.0	0.0075			
					0.6	1.681	0.0	0.0152			
					0.9	-	-	-			
				0.90 $\alpha=5.06°$	0.1	2.879	0.0	0.0028	0.0096	0.897	0.0049
					0.3	2.370	0.0	0.0077			
					0.6	1.943	0.0	0.0168			
					0.9	-	-	-			
NACA 0012 (standard)	0.45	90°	Upper	0.60 $\alpha=1.03°$	0.1	3.092	-0.011	0.0004	0.1	No	0.0084
					0.3	2.903	-0.039	0.0037			
					0.6	2.597	-0.074	0.0086			
					0.9	2.264	-0.109	0.0151			
				0.75 $\alpha=0.74°$	0.1	3.586	-0.011	0.0003	0.1	No	0.0109
					0.3	3.387	-0.017	0.0036			
					0.6	2.985	-0.037	0.0086			
					0.9	2.568	-0.068	0.0155			
				0.90 $\alpha=0.07°$	0.1	4.080	-0.011	0.0003	0.1	No	0.0136
					0.3	3.947	-0.003	0.0034			
					0.6	3.364	-0.015	0.0087			
					0.9	2.833	-0.046	0.0164			

TABLE I. — Continued

SUMMARY OF CALCULATED RESULTS

Case	μ	ψ	Surface	z/R	x/c	u_e	w_e	δ/c	Initial x/c	Separation x/c	T
NACA 0012 (standard)	0.45	90°	Lower	0.60 $\alpha=1.03°$	0.1	2.898	-0.011	0.0004	0.100	No	0.0081
					0.3	2.811	-0.022	0.0036			
					0.6	2.554	-0.046	0.0083			
					0.9	2.249	-0.077	0.0145			
				0.75 $\alpha=0.74°$	0.1	3.407	-0.011	0.0003	0.100	No	0.0106
					0.3	3.303	-0.017	0.0036			
					0.6	2.946	-0.037	0.0084			
					0.9	2.553	-0.068	0.0150			
				0.90 $\alpha=0.07°$	0.1	4.056	-0.011	0.0003	0.100	No	0.0136
					0.3	3.937	-0.004	0.0035			
					0.6	3.361	-0.016	0.0087			
					0.9	2.830	-0.048	0.0164			
NACA 0012 (standard)	0.23	90°	Upper	0.60 $\alpha=2.60°$	0.1	4.930	-0.018	0.0018	0.0381	No	0.0219
					0.3	4.460	-0.048	0.0054			
					0.6	3.972	-0.098	0.0108			
					0.9	3.465	-0.158	0.0183			
				0.75 $\alpha=2.29°$	0.1	5.832	-0.020	0.0018	0.0381	No	0.0304
					0.3	5.306	-0.050	0.0052			
					0.6	4.721	-0.099	0.0106			
					0.9	4.110	-0.157	0.0180			
				0.90 $\alpha=1.60°$	0.1	6.654	-0.023	0.0016	0.0381	No	0.0406
					0.3	6.156	-0.054	0.0048			
					0.6	5.493	-0.102	0.0100			
					0.9	4.792	-0.158	0.0170			

TABLE I. — Continued

SUMMARY OF CALCULATED RESULTS

Case	μ	ψ	Surface	z/R	x/c	u_e	w_e	δ/c	Initial x/c	Separation x/c	T
Advanced Airfoil	0.23	90°	Upper	0.60 $\alpha=2.60°$	0.1	5.302	-0.017	0.0016	0.0381	No	0.0243
					0.3	4.657	-0.041	0.0052			
					0.6	4.170	-0.089	0.0107			
					0.9	3.594	-0.146	0.0184			
				0.75 $\alpha=2.29°$	0.1	6.277	-0.018	0.0016	0.0381	No	0.0337
					0.3	5.537	-0.043	0.0050			
					0.6	4.953	-0.091	0.0105			
					0.9	4.258	-0.147	0.0182			
				0.90 $\alpha=1.60°$	0.1	7.167	-0.021	0.0014	0.0381	No	0.0445
					0.3	6.405	-0.048	0.0047			
					0.6	5.742	-0.096	0.0100			
					0.9	4.935	-0.151	0.0174			
NACA 0012 (2-D)	0.45	90°	Upper	0.60 $\alpha=1.03°$	0.1	3.090	0.0	0.0007	0.0843	No	0.0085
					0.3	2.901	0.0	0.0039			
					0.6	2.595	0.0	0.0089			
					0.9	2.263	0.0	0.0155			
				0.75 $\alpha=0.74°$	0.1	3.592	0.0	0.0007	0.0843	No	0.0111
					0.3	3.394	0.0	0.0038			
					0.6	2.992	0.0	0.0089			
					0.9	2.576	0.0	0.0159			
				0.90 $\alpha=0.07°$	0.1	4.119	0.0	0.0006	0.0843	No	0.0143
					0.3	3.987	0.0	0.0036			
					0.6	3.411	0.0	0.0089			
					0.9	2.888	0.0	0.0165			

TABLE I. — Continued

SUMMARY OF CALCULATED RESULTS

Case	μ	ψ	Surface	z/R	x/c	u_e	w_e	δ/c	Initial x/c	Separation x/c	T
NACA 0012 (standard)	0.45	180°	Upper	0.60 α=7.74°	0.1	2.150	-1.013	(0.0021)	0.0096	0.208	0.0007
					0.3	1.723	-1.032	(0.0071)	(0.0381)	0.941	0.0031
					0.6	0.421	-1.057	(0.0158)			
					0.9	1.151	-1.082	(0.031)			
				0.75 α=4.91°	0.1	2.491	-1.014	(0.0018)	0.0096	0.208	0.0017
					0.3	2.124	-1.035	(0.0060)	(0.0381)	0.941	0.0050
					0.6	1.823	-1.061	(0.0127)			
					0.9	1.540	-1.088	(0.0224)			
				0.90 α=2.46°	0.1	2.774	-1.016	(0.0017)	0.0096	0.208	0.0029
					0.3	2.509	-1.039	(0.0052)	(0.0381)	0.941	0.0071
					0.6	2.222	-1.067	(0.0109)			
					0.9	1.929	-1.094	(0.0187)			
NACA 0012 (standard)	0.45	180°	Lower	0.60 α=7.74°	0.1	0.936	-1.011	0.0008	0.100	No	0.0029
					0.3	1.251	-1.023	0.0043			
					0.6	1.310	-1.046	0.0087			
					0.9	1.273	-1.034	0.0136			
				0.75 α=4.91°	0.1	1.469	-1.011	0.0006	0.100	No	0.0044
					0.3	1.712	-1.021	0.0041			
					0.6	1.707	-1.043	0.0085			
					0.9	1.608	-1.072	0.0136			
				0.90 α=2.46°	0.1	2.100	-1.011	0.0005	0.100	No	0.0063
					0.3	2.225	-1.016	0.0037			
					0.6	2.127	-1.036	0.0084			
					0.9	1.946	-1.064	0.0139			

TABLE I. — Continued

SUMMARY OF CALCULATED RESULTS

Case	μ	ψ	Surface	z/R	x/c	u_e	w_e	δ/c	Initial x/c	Separation x/c	T
NACA 0012 (standard)	0.23	180°	Upper	0.60 $\alpha=9.58°$	0.1	4.404	-1.015	(0.0022)	0.0096	0.075	0.0015
					0.3	3.399	-1.041	(0.0078)	(0.0381)	0.869	0.0101
					0.6	2.714	-1.092	(0.0184)			
					0.9	-	-	-			
				0.75 $\alpha=8.24°$	0.1	5.370	-1.020	(0.0020)	0.0096	0.075	0.0026
					0.3	4.248	-1.051	(0.0070)	(0.0381)	0.869	0.0162
					0.6	3.453	-1.101	(0.0160)			
					0.9	-	-	-			
				0.90 $\alpha=5.42°$	0.1	5.981	-1.033	(0.0018)	0.0096	0.075	0.0042
					0.3	5.027	-1.079	(0.0059)	(0.0381)	0.869	0.0241
					0.6	4.264	-1.130	(0.0129)			
					0.9	-	-	-			
Advanced Airfoil	0.23	180°	Upper	0.60 $\alpha=9.58°$	0.1	4.719	-1.014	(0.0018)	0.0096	0.565	0.0066
					0.3	3.694	-1.035	(0.0067)	(0.0381)	0.958	0.0135
					0.6	3.069	-1.082	(0.0155)			
					0.9	2.472	-1.138	(0.0306)			
				0.75 $\alpha=8.24°$	0.1	5.756	-1.019	(0.0017)	0.0096	0.565	0.0138
					0.3	4.583	-1.046	(0.0062)	(0.0381)	0.958	0.0209
					0.6	3.848	-1.095	(0.0142)			
					0.9	3.129	-1.150	(0.0268)			
				0.90 $\alpha=5.42°$	0.1	6.418	-1.031	(0.0016)	0.0096	0.565	0.0255
					0.3	5.335	-1.076	(0.0055)	(0.0381)	0.958	0.0294
					0.6	4.603	-1.133	(0.0121)			
					0.9	3.839	-1.189	(0.0220)			

TABLE I. — Continued

SUMMARY OF CALCULATED RESULTS

Case	μ	ψ	Surface	z/R	x/c	u_e	w_e	δ/c	Initial x/c	Separation x/c	T
NACA 0012 (2-D)	0.45	180°	Upper	0.60	0.1	2.147	0.0	(0.0020)	0.0096	0.170	0.0006
				$\alpha=7.74°$	0.3	1.705	0.0	(0.0069)	(0.0381)	0.876	0.0025
					0.6	1.371	0.0	(0.0163)	(0.1)	0.963	0.0029
					0.9	-	-	-			
				0.75	0.1	2.481	0.0	(0.0018)	0.0096	0.170	0.0014
				$\alpha=4.91°$	0.3	2.109	0.0	(0.0058)	(0.0381)	0.876	0.0042
					0.6	1.786	0.0	(0.0127)	(0.1)	0.963	0.0044
					0.9	-	-	-			
				0.90	0.1	2.772	0.0	(0.0016)	0.0096	0.170	0.0023
				$\alpha=2.46°$	0.3	2.498	0.0	(0.0051)	(0.0381)	0.876	0.0063
					0.6	2.193	0.0	(0.0107)	(0.1)	0.963	0.0061
					0.9	-	-	-			
NACA 0012 (standard)	0.45	210°	Upper	0.60	0.1	1.624	-0.876	(0.0010)	0.0096	0.028	0.0001
				$\alpha=13.23°$	0.3	1.230	-0.892	(0.0062)	(0.0843)	0.914	0.0002
					0.6	0.991	-0.917	(0.0157)			
					0.9	0.797	-0.947	(0.0322)			
				0.75	0.1	2.047	-0.877	(0.0009)	0.0096	0.028	0.0002
				$\alpha=9.33°$	0.3	1.632	-0.898	(0.0054)	(0.0843)	0.914	0.0008
					0.6	1.358	-0.927	(0.0129)			
					0.9	1.124	-0.958	(0.0244)			
				0.90	0.1	2.304	-0.878	(0.0008)	0.0096	0.028	0.0003
				$\alpha=5.25°$	0.3	1.967	-0.905	(0.0047)	(0.0843)	0.914	0.0018
					0.6	1.700	-0.939	(0.0110)			
					0.9	1.451	-0.973	(0.0197)			

TABLE I. — Continued

SUMMARY OF CALCULATED RESULTS

Case	μ	ψ	Surface	z/R	x/c	u_e	w_e	δ/c	Initial x/c	Separation x/c	T
NACA 0012 (standard)	0.45	240°	Upper	0.60	0.1	0.981	-0.509	(0.0015)	0.0096	0.020	0.0000
			α=16.46°		0.3	0.722	-0.516	(0.0076)	(0.0843)	0.899	0.0005
					0.6	0.575	-0.538	(0.0193)			
					0.9	-	-	-			
				0.75	0.1	1.565	-0.510	(0.0011)	0.0096	0.020	0.0001
			α=13.93°		0.3	1.181	-0.523	(0.0061)	(0.0843)	0.899	0.0013
					0.6	0.949	-0.549	(0.0154)			
					0.9	-	-	-			
				0.90	0.1	1.929	-0.512	(0.0009)			
			α=8.46°		0.3	1.558	-0.538	(0.0052)	0.0096	0.020	0.0001
					0.6	1.305	-0.572	(0.0123)	(0.0843)	0.899	0.0023
					0.9	-	-	-			
NACA 0012 (standard)	0.45	240°	Lower	0.60	0.1	0.089	-0.511	0.0022	0.100	No	0.0004
			α=16.46°		0.3	0.293	-0.538	0.0062			
					0.6	0.367	-0.570	0.0109			
					0.9	0.391	-0.599	0.0158			
				0.75	0.1	0.291	-0.511	0.0020	0.100	No	0.0009
			α=13.93°		0.3	0.603	-0.535	0.0039			
					0.6	0.702	-0.567	0.0073			
					0.9	0.722	-0.600	0.0117			
				0.90	0.1	0.751	-0.511	0.0013	0.100	No	0.0019
			α=8.46°		0.3	1.041	-0.520	0.0035			
					0.6	1.104	-0.539	0.0072			
					0.9	1.085	-0.563	0.0117			

TABLE I. — Continued

SUMMARY OF CALCULATED RESULTS

Case	μ	ψ	Surface	z/R	x/c	u_e	w_e	δ/c	Initial x/c	Separation x/c	T
NACA 0012 (standard)	0.23	240°	Upper $\alpha{=}16.59°$	0.60	0.1	3.696	-0.519	(0.0010)	0.0096	0.020	0.0005
					0.3	2.678	-0.539	(0.0064)	(0.038)	0.725	0.00530
					0.6	2.081	-0.585	(0.0172)	(0.084)	0.871	0.00563
					0.9	-	-	-			
			$\alpha{=}13.70°$	0.75	0.1	4.767	-0.520	(0.0009)	0.0096	0.020	0.0008
					0.3	3.568	-0.549	(0.0056)	(0.038)	0.725	0.01035
					0.6	2.838	-0.599	(0.0146)	(0.084)	0.871	0.01038
					0.9	-	-	-			
			$\alpha{=}10.05°$	0.90	0.1	5.521	-0.522	(0.0008)	0.0096	0.020	0.0011
					0.3	4.338	-0.564	(0.0050)	(0.038)	0.725	0.01662
					0.6	3.564	-0.622	(0.0125)	(0.084)	0.871	0.01601
					0.9	-	-	-			
Advanced Airfoil	0.23	240°	Upper $\alpha{=}16.59°$	0.60	0.1	3.670	-0.510	(0.0021)	0.0096	0.044	0.0005
					0.3	2.610	-0.528	(0.0091)	(0.0215)	0.293	0.0031
					0.6	1.995	-0.573	(0.0250)	(0.0381)	0.725	0.0053
					0.9	-	-	-			
			$\alpha{=}13.70°$	0.75	0.1	4.785	-0.515	(0.0019)	0.0096	0.044	0.0012
					0.3	3.525	-0.539	(0.0077)	(0.0215)	0.293	0.0064
					0.6	2.781	-0.586	(0.0192)	(0.0381)	0.725	0.0104
					0.9	-	-	-			
			$\alpha{=}10.05°$	0.90	0.1	5.631	-0.524	(0.0017)	0.0096	0.044	0.0019
					0.3	4.357	-0.559	(0.0066)	(0.0215)	0.293	0.0104
					0.6	3.579	-0.609	(0.0154)	(0.0381)	0.725	0.0166
					0.9	-	-	-			

TABLE I. — Continued

SUMMARY OF CALCULATED RESULTS

Case	μ	ψ	Surface	z/R	x/c	u_e	w_e	δ/c	Initial x/c	Separation x/c	T
NACA 0012 (yawed wing)	0.45	240°	Upper α=16.46°	0.60	0.1	0.986	-0.511	(0.0010)	0.0096	0.020	0.0000
					0.3	0.730	-0.518	(0.0069)	(0.1)	0.936	0.0006
					0.6	0.585	-0.539	(0.0186)			
					0.9	0.471	-0.569	(0.0408)			
				0.75 α=13.93°	0.1	1.573	-0.511	(0.0007)	0.0096	0.020	0.0001
					0.3	1.193	-0.524	(0.0056)	(0.1)	0.936	0.0013
					0.6	0.964	-0.550	(0.0145)			
					0.9	0.779	-0.580	(0.0301)			
				0.90 α=8.46°	0.1	1.937	-0.511	(0.0006)	0.0096	0.020	0.0001
					0.3	1.569	-0.537	(0.0048)	(0.1)	0.936	0.0024
					0.6	1.318	-0.571	(0.0118)			
					0.9	1.099	-0.605	(0.0228)			
NACA 0012 (yawed wing)	0.45	240°	Lower α=16.46°	0.60	0.1	0.085	-0.512	0.0028	0.084	No	0.0004
					0.3	0.292	-0.538	0.0072			
					0.6	0.367	-0.570	0.0129			
					0.9	0.391	-0.599	0.0197			
				0.75 α=13.93°	0.1	0.297	-0.511	0.0020	0.084	No	0.0010
					0.3	0.607	-0.535	0.0039			
					0.6	0.706	-0.567	0.0079			
					0.9	0.727	-0.600	0.0123			
				0.90 α=8.46°	0.1	0.760	-0.510	0.0015	0.084	No	0.0020
					0.3	1.048	-0.518	0.0037			
					0.6	1.112	-0.537	0.0071			
					0.9	1.093	-0.561	0.0118			

TABLE I. — Continued

SUMMARY OF CALCULATED RESULTS

Case	μ	ψ	Surface	z/R	x/c	u_e	w_e	δ/c	Initial x/c	Separation x/c	T
NACA 0012 (2-D)	0.45	240°	Upper $\alpha=16.46°$	0.60	0.1	0.986	0.0	(0.0010)	0.0096	0.019	0.0000
					0.3	0.704	0.0	(0.0068)	(0.1)	0.666	0.0003
					0.6	0.515	0.0	(0.0215)			
					0.9	–	–	–			
				0.75	0.1	1.573	0.0	(0.0007)	0.0096	0.019	0.0001
			$\alpha=13.93°$		0.3	1.180	0.0	(0.0054)	(0.1)	0.666	0.0010
					0.6	0.928	0.0	(0.0148)			
					0.9	–	–	–			
				0.90	0.1	1.937	0.0	(0.0006)	0.0096	0.019	0.0001
			$\alpha=8.46°$		0.3	1.563	0.0	(0.0047)	(0.1)	0.666	0.0019
					0.6	1.301	0.0	(0.0117)			
					0.9	–	–	–			
NACA 0012 (standard)	0.45	270°	Upper $\alpha=12.76°$	0.60	0.1	0.634	-0.009	(0.0022)	0.0096	0.020	0.0000
					0.3	0.483	-0.015	(0.0083)	(0.0843)	0.914	0.0002
					0.6	0.392	-0.037	(0.0194)			
					0.9	0.320	-0.068	(0.0381)			
				0.75	0.1	1.303	-0.009	(0.0012)			
			$\alpha=13.55°$		0.3	0.979	-0.019	(0.0064)	0.0096	0.020	0.0001
					0.6	0.782	-0.043	(0.0162)	(0.0843)	0.914	0.0008
					0.9	0.623	-0.073	(0.0346)			
				0.90	0.1	1.752	-0.011	(0.0009)	0.0096	0.020	0.0001
			$\alpha=9.50°$		0.3	1.394	-0.032	(0.0053)	0.0843	0.914	0.00018
					0.6	1.157	-0.061	(0.0128)			
					0.9	0.955	-0.092	(0.0244)			

TABLE I. — Continued

SUMMARY OF CALCULATED RESULTS

Case	μ	ψ	Surface	z/R	x/c	u_e	w_e	δ/c	Initial x/c	Separation x/c	T
NACA 0012 (standard)	0.45	270°	Lower	0.60 $\alpha=12.76°$	0.1	0.141	-0.013	0.0071	0.084	No	0.0002
					0.3	0.260	-0.046	0.0042			
					0.6	0.293	-0.086	0.0077			
					0.9	0.296	-0.122	0.0120			
				0.75 $\alpha=13.55°$	0.1	0.245	-0.012	0.0039	0.084	No	0.0006
					0.3	0.504	-0.041	0.0028			
					0.6	0.584	-0.077	0.0064			
					0.9	0.600	-0.111	0.0100			
				0.90 $\alpha=9.50°$	0.1	0.609	-0.010	0.0019	0.084	No	0.0014
					0.3	0.888	-0.024	0.0032			
					0.6	0.952	-0.048	0.0067			
					0.9	0.941	-0.076	0.0107			
NACA 0012 (standard)	0.23	270°	Upper	0.60 $\alpha=16.42°$	0.1	3.410	-0.021	(0.0008)	0.0096 (0.1)	0.021 0.894	0.0004 0.0048
					0.3	2.485	-0.042	(0.0058)			
					0.6	1.943	-0.088	(0.0158)			
					0.9	-	-	-			
				0.75 $\alpha=13.36°$	0.1	4.470	-0.021	(0.0006)	0.0096 (0.1)	0.021 0.894	0.0007 0.0093
					0.3	3.373	-0.051	(0.0051)			
					0.6	2.704	-0.101	(0.0135)			
					0.9	-	-	-			
				0.90 $\alpha=9.92°$	0.1	5.261	-0.021	(0.0005)	0.0096 (0.1)	0.021 0.894	0.0010 0.0149
					0.3	4.156	-0.060	(0.0046)			
					0.6	3.433	-0.115	(0.0117)			
					0.9	-	-	-			

TABLE I. — Concluded

SUMMARY OF CALCULATED RESULTS

Case	μ	ψ	Surface	z/R	x/c	u_e	w_e	δ/c	Initial x/c	Separation x/c	T
NACA 0012 (standard)	0.45	300°	Upper	0.60 α=6.28°	0.1	0.724	0.491	(0.0018)	0.0096	0.045	0.0000
					0.3	0.599	0.486	(0.0073)	(0.0843)	0.955	0.0005
					0.6	0.505	0.467	(0.0162)			
					0.9	0.423	0.441	(0.0296)			
				0.75 α=9.58°	0.1	1.397	0.491	(0.0011)	0.0096	0.045	0.0001
					0.3	1.104	0.484	(0.0059)	(0.0843)	0.955	0.0012
					0.6	0.909	0.462	(0.0142)			
					0.9	0.745	0.432	(0.0274)			
				0.90 α=8.62°	0.1	1.940	0.490	(0.0009)	0.0096	0.045	0.0002
					0.3	1.561	0.474	(0.0052)	(0.0843)	0.955	0.0023
					0.6	1.303	0.447	(0.0125)			
					0.9	1.080	0.418	(0.0240)			
NACA 0012 (standard)	0.45	330°	Upper	0.60 α=3.94°	0.1	1.162	0.863	(0.0025)	0.0096	0.249	0.0006
					0.3	1.009	0.854	(0.0075)	(0.0381)	0.929	0.0014
					0.6	0.879	0.830	(0.0152)			
					0.9	0.756	0.796	(0.0256)			
				0.75 α=6.76°	0.1	1.805	0.862	(0.0022)	0.0096	0.249	0.0007
					0.3	1.469	0.855	(0.0072)	(0.0381)	0.929	0.0024
					0.6	1.222	0.828	(0.0156)			
					0.9	1.000	0.791	(0.0301)			
				0.90 α=6.72°	0.1	2.358	0.857	(0.0019)	0.0096	0.249	0.0012
					0.3	1.922	0.843	(0.0066)	(0.0381)	0.929	0.0037
					0.6	1.594	0.818	(0.0149)			
					0.9	1.294	0.788	(0.0295)			

APPENDIX

SIKORSKY H-34 HELICOPTER ROTOR; ANGLES OF ATTACK

Figures A-1 and A-2 show the spanwise variation of angle of attack for various azimuthal positions for the H-34 Sikorsky helicopter rotor. These curves were derived by Dr. W. J. McCroskey of the U. S. Army Aeronautical Research Laboratory and were used in the present calculations.

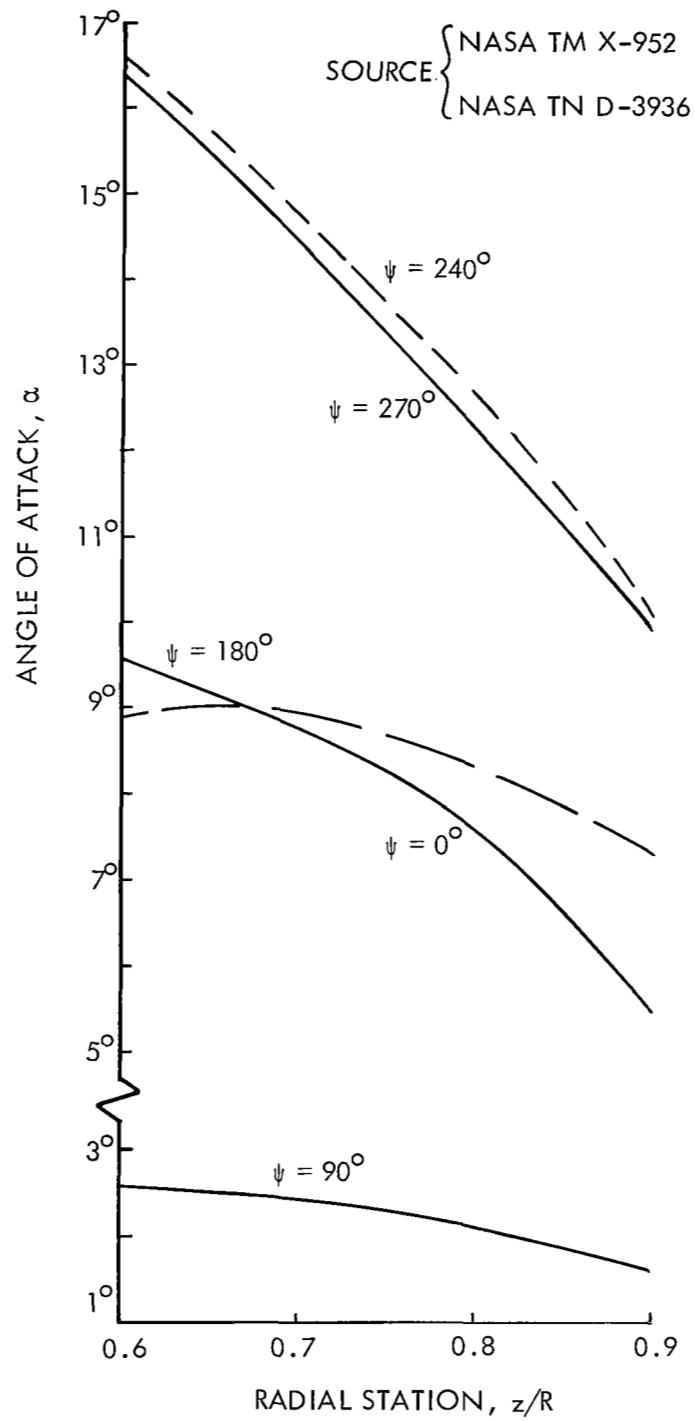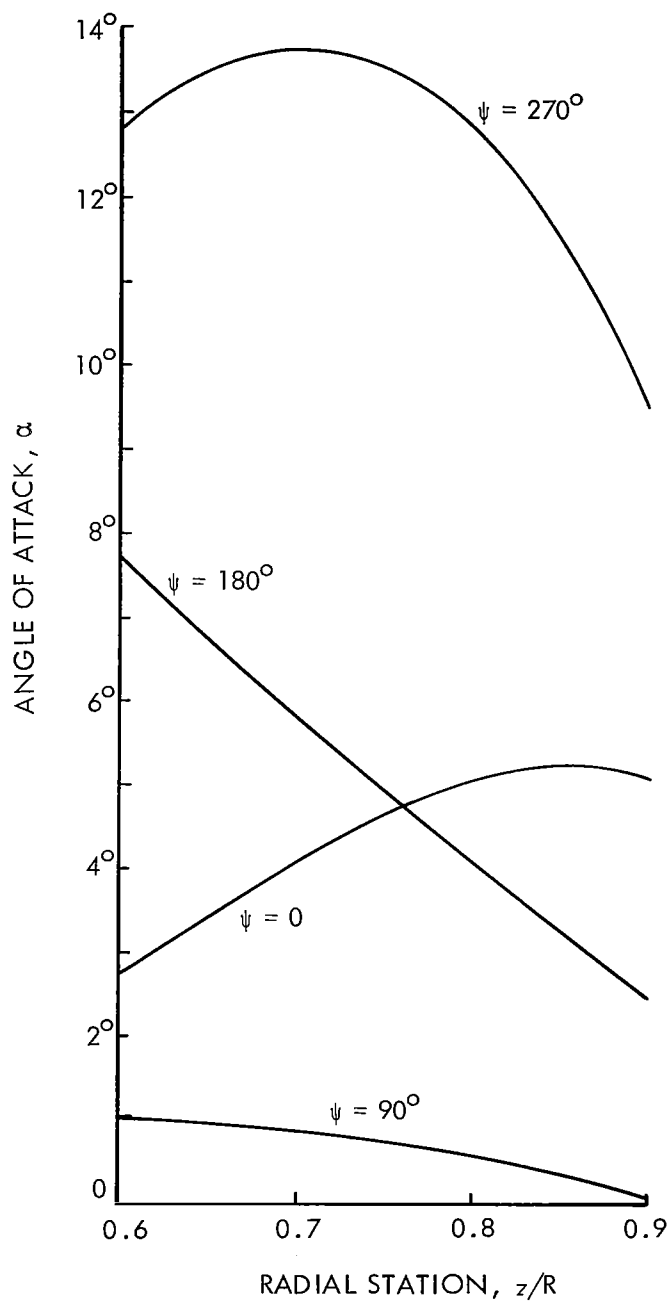A polar plot of the local angle of attack, for an advance ratio, μ, of 0.45, is shown in figure A-3.

FIGURE A-1. H-34 ROTOR ANGLES OF ATTACK FOR μ = 0.23.

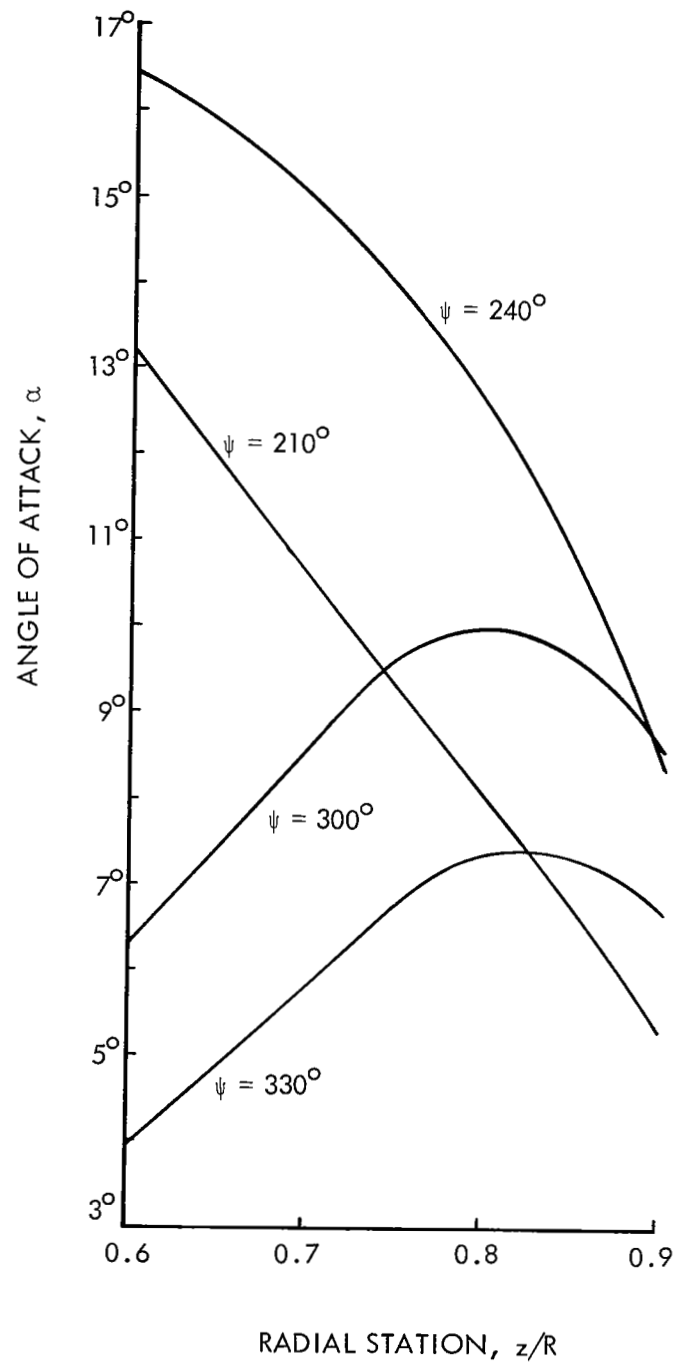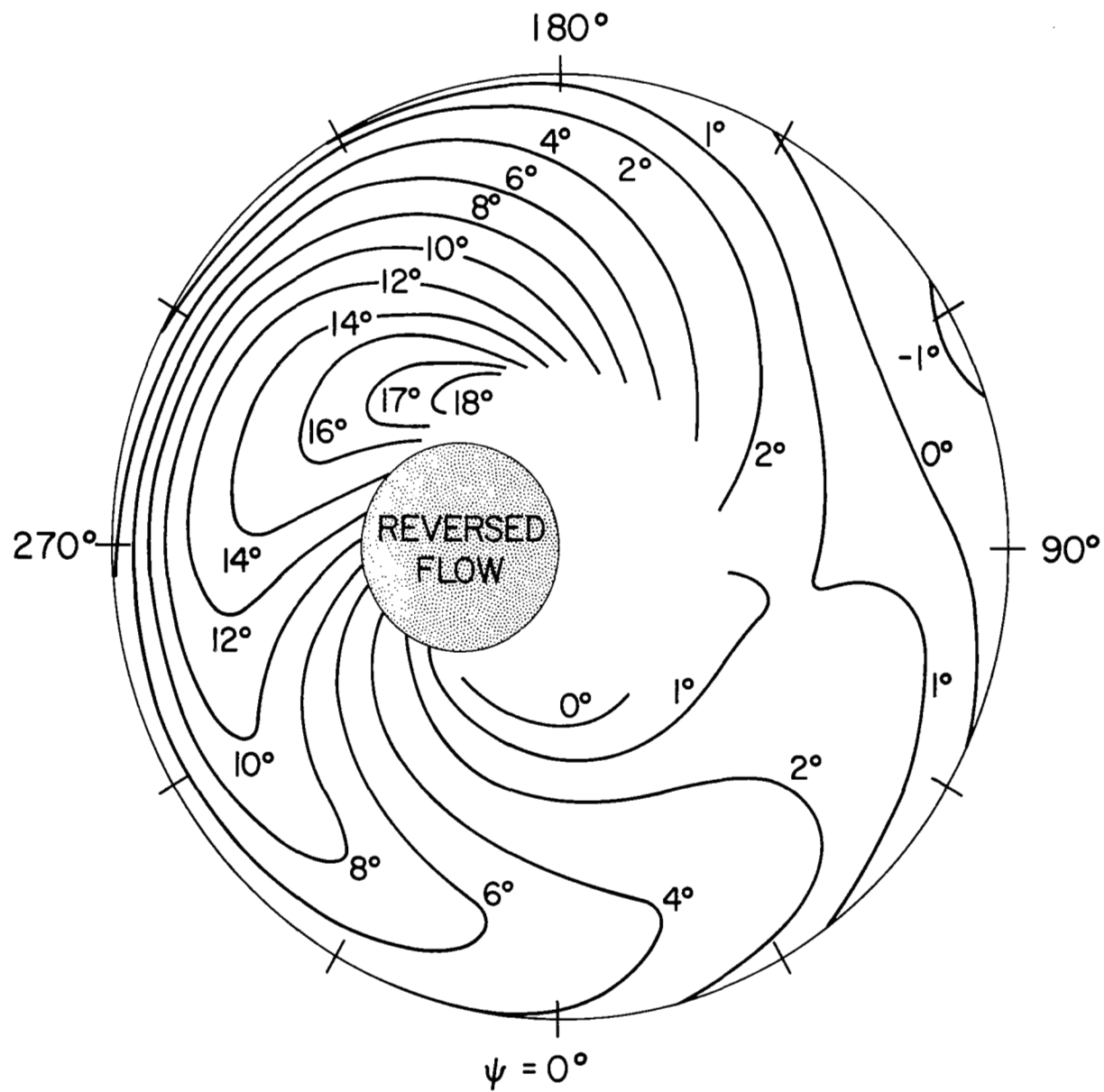FIGURE A-2. H-34 ROTOR ANGLES OF ATTACK FOR μ = 0.45.

FIGURE A-2. (CONTINUED)

FIGURE A-3. POLAR PLOT OF LOCAL ANGLES OF ATTACK FOR $\mu = 0.45$

REFERENCES

1. McCroskey, W. J., and Yaggy, P. F.: Laminar Boundary Layers on Helicopter Rotors in Forward Flight. AIAA Journal, vol. 6, no. 16, October 1968, p. 1919.

2. Dwyer, H. A., and McCroskey, W. J.: Paper 70-50 presented at AIAA 8th Aerospace Sciences Meeting (New York), January 1970.

3. Weber, J.: The Calculation of the Pressure Distribution over the Surface of Two-Dimensional and Swepth Wings with Symmetrical Aerofoil Sections. R & M 2819, British Aero. Res. Council, July 1953.

4. Weber, J.: The Calculation of the Pressure Distribution on the Surface of Cambered Wings and the Design of Wings with Given Pressure Distribution. R & M 3026, British Aero. Res. Council, 1955.

5. Nash, J. F.: The Calculation of Three-Dimensional Turbulent Boundary Layers in Incompressible Flow. J. of Fluid Mechanics, vol. 37, part 4, 1969, pp. 625-642.

6. McCroskey, W. J., Nash, J. F., and Hicks, J. G.: Turbulent Boundary Layer Flow over a Rotating Flat-Plate Blade. (Paper to be published.)

7. Rabbot, J.: A Presentation of Measured and Calculated Full Scale Rotor Blade Aerodynamic and Structural Loads. Tech. Rep. 66-31, USAAVLABS, 1966.

8. Scheiman, J., and Kelley, H. L.: Comparison of Flight-Measured Helicopter Rotor-Blade Chordwise Pressure Distributions with Static Two-Dimensional Airfoil Characteristics. NASA TN-D-3936, May 1967.

9. Nash, J. F., and Tseng, R. R.: The Three-Dimensional Turbulent Boundary Layer on an Infinite Yawed Wing. (Paper to be published.)

10. Abbot, I. H., and von Doenhoff, A. E.: Theory of Wing Sections. Dover Publications, Inc. (New York), 1959.

11. Bradshaw, P., Ferris, D. H., and Atwell, N. P.: Calculation of Boundary-Layer Development Using the Turbulent Energy Equation. J. Fluid Mechanics, vol. 28, part 3, May 1967, p. 593.

12. McCullough, G. B., and Gault, D. E.: Examples of Three Representative Types of Airfoil-Section Stall at Low Speed. NACA TN 2502, September 1951.